atoms

MDPI

Review

Multiconfiguration Dirac-Hartree-Fock Calculations with Spectroscopic Accuracy: Applications to Astrophysics

Per Jönsson [1,*], Gediminas Gaigalas [2], Pavel Rynkun [2], Laima Radžiūtė [2], Jörgen Ekman [1], Stefan Gustafsson [1], Henrik Hartman [1], Kai Wang [1], Michel Godefroid [3], Charlotte Froese Fischer [4], Ian Grant [5,6], Tomas Brage [7] and Giulio Del Zanna [6]

1 Materials Science and Applied Mathematics, Malmö University, SE-205 06 Malmö, Sweden; jorgen.ekman@mah.se (J.E.); stefan.gustafsson@mah.se (S.G.); henrik.hartman@mah.se (H.H.); kaiwang1128@aliyun.com (K.W.)

2 Institute of Theoretical Physics and Astronomy, Vilnius University, Saulėtekio av. 3, LT-10222 Vilnius, Lithuania; Gediminas.Gaigalas@tfai.vu.lt (G.G.); pavel.rynkun@gmail.com (P.R.); laima.radziute@gmail.com (L.R.)

3 Chimie Quantique et Photophysique, Université libre de Bruxelles, B-1050 Brussels, Belgium; michel.godefroid@ulb.ac.be

4 Department of Computer Science, University of British Columbia, Vancouver, BC V6T 1Z4, Canada; cff@cs.ubc.ca

5 Mathematical Institute, University of Oxford, Woodstock Road, Oxford OX2 6GG, UK; iangrant15@btinternet.com

6 Department of Applied Mathematics and Theoretical Physics, Centre for Mathematical Sciences, University of Cambridge, Wilberforce Road, Cambridge CB3 0WA, UK; gd232@cam.ac.uk

7 Division of Mathematical Physics, Department of Physics, Lund University, 221-00 Lund, Sweden; tomas.brage@fysik.lu.se

* Correspondence: per.jonsson@mah.se; Tel.: +46-40-66-57251

Academic Editor: Joseph Reader
Received: 31 January 2017; Accepted: 7 April 2017; Published: 14 April 2017

Abstract: Atomic data, such as wavelengths, spectroscopic labels, broadening parameters and transition rates, are necessary for many applications, especially in plasma diagnostics, and for interpreting the spectra of distant astrophysical objects. The experiment with its limited resources is unlikely to ever be able to provide a complete dataset on any atomic system. Instead, the bulk of the data must be calculated. Based on fundamental principles and well-justified approximations, theoretical atomic physics derives and implements algorithms and computational procedures that yield the desired data. We review progress and recent developments in fully-relativistic multiconfiguration Dirac–Hartree–Fock methods and show how large-scale calculations can give transition energies of spectroscopic accuracy, i.e., with an accuracy comparable to the one obtained from observations, as well as transition rates with estimated uncertainties of a few percent for a broad range of ions. Finally, we discuss further developments and challenges.

Keywords: transition energies; lifetimes; transition rates; multiconfiguration Dirac-Hartree-Fock

PACS: 31.15.am; 32.30.Jc; 32.70.Cs

1. Introduction

Atomic data, such as wavelengths, spectroscopic labels, broadening parameters, excitation and transition rates, are necessary for many applications, especially in plasma diagnostics, and for interpreting laboratory and astrophysical spectra [1,2]. Plasma diagnostics are commonly applied to

measure the physical state of the plasma, e.g., temperatures, densities, ion and chemical abundances. Atomic databases, such as CHIANTI [3,4], are widely used for such diagnostic purposes. Their accuracy relies on a range of atomic rates, the main ones being electron collision rates and transition rates. For the solar corona, lines from highly charged iron ions, emitted in the extreme ultraviolet (EUV) and soft X-ray region, are commonly used for diagnostics, together with those from all other abundant elements. Atomic data and line identifications involving states of the lowest configurations of an ion are now relatively well known and observed. However, much less data are available for lines from higher configurations; one example is the lack of line identifications and rates for transitions from $n = 4$ iron ions in the soft X-rays [5].

Line identification from observed spectra is a very difficult and challenging task. Different methods such as isoelectronic interpolation and extrapolation, perfected by Edlén [6], can be used, but the work is nowadays mostly done with the aid of calculated transition energies and simulated spectra. For calculated transition energies, or wavelengths, to be of practical use, they need to be very accurate with uncertainties of just a few mÅ, placing high demands on computational methodologies.

Transition rates and line ratios are needed for diagnostic purposes. Due to the almost complete lack of accurate experimental data for atoms a few times ionized or more, the bulk of the transition rates must be calculated. Not only the rates themselves should be provided, but also uncertainty estimates that can be propagated in plasma models for sensitivity analysis. Both accurate rates and uncertainty estimates pose a challenge, calling for methods for which computed properties can be monitored as the wave functions are systematically improved.

This review summarizes the results from recent accurate relativistic multiconfiguration calculations for lowly charged ions or more of astrophysical importance. Focus is on the transition energies and their uncertainties, but transition rates and the associated uncertainty estimates are also discussed. The astrophysical background is provided in the individual papers covered by the review. Neutral atoms and ions in the lowest charge states are not covered in the review.

2. Multiconfiguration Methods

Multiconfiguration methods are versatile and can, in principle, be applied to any atomic or ionic system [7]. Multiconfiguration methods generate approximate energies and wave functions for the each of the targeted states in a system. The wave functions can then be used to compute measurable quantities, such as transition rates, hyperfine structures or Landé g-factors [8]. Looking at strengths and weaknesses, multiconfiguration methods capture near degeneracies and valence-valence electron correlation very efficiently. They are however less good at accounting for core-core correlation, and here, perturbative methods relying on a complete orbital basis have advantages. Work has been done to combine multiconfiguration and perturbative methods in different ways [9–12], a development that will open up accurate results also for more complex systems [13].

The relativistic multiconfiguration method, to be described below, is implemented in the GRASP2K program package [14]. The package is generally available and utilizes a message passing interface (MPI) for the most time-consuming programs, allowing for large-scale computing on parallel computers.

2.1. Multiconfiguration Dirac-Hartree-Fock

Atomic calculations are based on a Hamiltonian. In the relativistic multiconfiguration Dirac-Hartree-Fock (RMCDHF) method [7,15], as implemented in the GRASP2K package, the Hamiltonian is taken as the Dirac-Coulomb Hamiltonian:

$$H_{\mathrm{DC}} = \sum_{i=1}^{N} \left(c\,\boldsymbol{\alpha}_i \cdot \boldsymbol{p}_i + (\beta_i - 1)c^2 + V_{\mathrm{nuc}}(r_i) \right) + \sum_{i>j}^{N} \frac{1}{r_{ij}}, \tag{1}$$

where $V_{\rm nuc}(r_i)$ is the nuclear potential modelled from an extended nuclear charge distribution, r_{ij} is the distance between electrons i and j and $\boldsymbol{\alpha}$ and β are the Dirac matrices. Wave functions $\Psi(\gamma PJM_J)$ for fine-structure states labelled by parity, P, and angular quantum numbers, JM_J, are expanded in antisymmetrized and coupled configuration state functions (CSFs):

$$\Psi(\gamma PJM_J) = \sum_{j=1}^{N_{\rm CSF}} c_j \Phi(\gamma_j PJM_J). \tag{2}$$

The labels $\{\gamma_j\}$ denote the information of the CSFs, such as orbital occupancy and subshell quantum numbers in the angular momentum coupling tree. The CSFs are built from products of one-electron orbitals, having the general form:

$$\psi_{n\kappa,m}(\mathbf{r}) = \frac{1}{r}\begin{pmatrix} P_{n\kappa}(r)\chi_{\kappa,m}(\theta,\varphi) \\ \imath Q_{n\kappa}(r)\chi_{-\kappa,m}(\theta,\varphi) \end{pmatrix}, \tag{3}$$

where $\chi_{\pm\kappa,m}(\theta,\varphi)$ are two-component spin-orbit functions and where the radial functions are numerically represented on a logarithmic grid. The selection of the CSFs depends on the atomic system at hand and is described in Section 3.

In applications, one often seeks to determine energies and wave functions for a number, sometimes up to a few hundred, of targeted states. This is most conveniently done in the extended optimal level (EOL) scheme [16]. Given initial estimates of the radial functions, the energies E and expansion coefficients $c = (c_1, \ldots, c_M)^t$ for the targeted states are obtained as solutions to the relativistic configuration interaction (RCI) problem:

$$Hc = E\mathbf{c}, \tag{4}$$

where H is the RCI matrix of dimension $M \times M$ with elements:

$$H_{ij} = \langle \Phi(\gamma_i PJM_J)|H_{\rm DC}|\Phi(\gamma_j PJM_J)\rangle. \tag{5}$$

Once the expansion coefficients have been determined, the radial functions $\{P_{n\kappa}(r), Q_{n\kappa}(r)\}$ are improved by solving a set of differential equations that results from applying the variational principle on a weighted energy functional of the targeted states together with additional terms needed to preserve the orthonormality of the orbitals. Appropriate boundary conditions for the radial orbitals exclude undesired negative-energy solutions [15]. The RCI problem and the solution of the differential equations are iterated until the radial orbitals and the energy are converged to a specified tolerance.

2.2. Configuration Interaction

The RMCDHF calculations are used to generate an orbital basis. Given this basis, the final wave functions for the targeted states are obtained in RCI calculations based on the frequency dependent Dirac-Coulomb-Breit Hamiltonian:

$$H_{\rm DCB} = H_{\rm DC} - \sum_{i<j}^{N}\left[\boldsymbol{\alpha}_i\cdot\boldsymbol{\alpha}_j\frac{\cos(\omega_{ij}r_{ij}/c)}{r_{ij}} + (\boldsymbol{\alpha}_i\cdot\boldsymbol{\nabla})(\boldsymbol{\alpha}_j\cdot\boldsymbol{\nabla})\frac{\cos(\omega_{ij}r_{ij}/c)-1}{\omega_{ij}^2 r_{ij}/c^2}\right], \tag{6}$$

where $\boldsymbol{\nabla}$ is the gradient operator involving differentiation with respect to $\mathbf{r}_{ij} = \mathbf{r}_i - \mathbf{r}_j$ and $r_{ij} = |\mathbf{r}_{ij}|$ [17]. In the RCI calculations leading quantum electrodynamic (QED) effects, vacuum polarization and self-energy are also taken into account. RCI calculations require less computational effort than do RMCDHF calculations, and currently, expansions with millions of CSFs can be handled. The relativistic multiconfiguration and configuration interaction calculations go together and are referred to as RMCDHF/RCI calculations.

2.3. Managing Large Expansions

To manage large expansions, CSFs can a priori be divided into two groups, referred to as a zero- and first-order partitioning. The first group, P, with m elements ($m \ll M$) contains CSFs that account for the major parts of the wave functions. The second group, Q, with $M - m$ elements contains CSFs that represent minor corrections. Allowing interaction between CSFs in group P, interaction between CSFs in groups P and Q and diagonal interactions between CSFs in Q gives a matrix:

$$\begin{pmatrix} H^{(PP)} & H^{(PQ)} \\ H^{(QP)} & H^{(QQ)} \end{pmatrix}, \tag{7}$$

where $H_{ij}^{(QQ)} = \delta_{ij} E_i^Q$. The restriction of $H^{(QQ)}$ to diagonal elements results in a huge reduction in the total number of matrix elements and the corresponding time for RCI calculations [12]. A similar reduction in computational time is obtained when constructing and solving the differential equations obtained from the weighted energy functional. Different computational strategies apply: RMCDHF calculations with limited interactions followed by RCI calculations with full interactions or RMCDHF calculations with limited interactions followed by RCI calculations with limited interaction, possibly with more CSFs in group P.

2.4. Labelling

In fully-relativistic calculations, quantum labels for the targeted states are obtained in jj-coupling. Most often, this wave function representation is not pure, i.e., there is no dominant CSF whose quantum numbers can be used to label a state in a proper way. Using the methods developed by Gaigalas and co-workers [18], the wave function representation in jj-coupling is transformed to an approximate representation in LSJ-coupling. This representation is normally more pure and better suited for labelling. One should be aware of the fact that even in LSJ-coupling, the labelling is not straight forward, and several components in the LSJ-coupling representation must be used in a recursive way to find unique labels [19,20]. Programs for transforming wave functions and assigning unique labels are important parts of the GRASP2K package [21].

2.5. Transition Properties

Given wave functions from RMCDHF/RCI calculations, transition properties, such as rates, A, line strengths, S, and weighted oscillator strengths, gf, between two states γPJ and $\gamma' P' J'$ are computed in terms of reduced matrix elements:

$$\langle\, \Psi(\gamma PJ) \,\|T^{(\mathrm{EMK})}\|\, \Psi(\gamma' P' J') \,\rangle, \tag{8}$$

where the operator $T^{(\mathrm{EMK})}$ depends on the multipolarity, E1, M1, E2, M2, etc., of the transition. By including Bessel functions in the definition of the operator, GRASP2K accounts for more high-order effects than the usual transition operator used in non-relativistic calculations with Breit–Pauli corrections [15]. Inserting the CSF expansions for the wave functions, the reduced matrix element reduces to a sum over reduced matrix elements between CSFs. Using Racah algebra techniques, these matrix elements are finally obtained as sums over radial integrals [22,23]. The above procedure assumes that the two states γPJ and $\gamma' P' J'$ are built from the same set of orbitals. When this is not the case, e.g., when separate calculations have been done for the even and odd parity states, the representation of the wave functions are changed in such a way that the orbitals become biorthonormal [24,25], in which case the calculation continues along the lines above. For electric transitions, parameters can be computed in both length and velocity gauge [26], where the results in the length gauge are the preferred.

3. General Computational Methodology: The SD-MR Approach

Systematic calculations using multiconfiguration methods follow a determined scheme as described below. Details of the scheme are determined by the shell structure of the atom, the number of targeted states, the desired accuracy of the final results and the available computational resources. The atomic Hamiltonian is invariant with respect to space inversions, and there are no interactions between odd and even parity states. The odd and even parity states are thus often treated in separate sets of calculations. After validation for selected ions and states, computed transition energies and rates can be used to aid the analysis of unknown spectra.

3.1. Multireference and Gross Features of the Wave Functions

For highly ionized systems, a natural starting point is the multireference set (MR). In this review, we define the MR as the set of configurations associated with the targeted states of a given parity together with important closely degenerate configurations. Applying rules for the coupling of angular momenta, the configurations in the MR give rise to a set of CSFs that account for the most important gross features of the wave functions. The expansion coefficients of the CSFs and the orbitals are determined in an initial RMCDHF calculation. The orbitals for the initial calculation are called spectroscopic orbitals. They are required to have the same node structure as hydrogenic orbitals, i.e., the node structure is determined by the principal quantum number. The spectroscopic orbitals are kept frozen in all subsequent calculations.

3.2. Including Electron Correlation and Determining an Orbital Set

The initial approximation of the wave functions is improved by adding CSFs that account for electron correlation. Guided by a perturbative analysis, the CSFs are generated by the single (S) and double (D) multireference (SD-MR) active space method in which a number of configurations is obtained by SD substitutions of orbitals in the configurations of the MR with orbitals in an active set [7,8]. Again, applying rules for the coupling of angular momenta, the generated configurations give rise to the CSFs. Not all of these CSFs are important, and the CSFs are further required to be such that they interact (have non-zero Hamiltonian matrix elements) with the CSFs of the MR. The expansion coefficients of the CSFs and the radial parts of the orbitals in the active set are determined in RMCDHF calculations where, for large expansions, limited interactions are used.

The active set, often denoted by the number of orbitals with a specified symmetry, so that $\{4s3p2d1f\}$ is a set with four s orbitals, three p orbitals, two d orbitals and one f orbital, is systematically enlarged one orbital layer at the time until the computed excitation energies and transition rates have converged to within some predetermined tolerance. For small systems, SD substitutions are done from all subshells of the configurations in the MR, and the generated CSFs account for valence-valence, core-valence and core-core electron correlation. For larger systems, it becomes necessary to define a core for which restrictions on the substitutions apply. In many cases, the SD-MR substitutions are restricted in such a way that there are only S substitutions from subshells that define a so-called active core. There may also be subshells deep down in the core for which there are no substitutions at all. CSFs obtained from S-MR substitutions from the active core together with SD-MR substitutions from the valence subshells account for valence-valence and core-valence correlation.

3.3. Final Configuration Interaction Calculations Including the Breit Interaction and QED Effects

The frequency dependent Breit (transverse photon) interaction and leading QED effects are included in final RCI calculations. To account for higher order correlation effects, the MR is sometimes enlarged at this final step leading to larger expansions. Full interaction is normally used, although limited interactions have been shown effective for including core-valence and core-core effects in larger systems [12,27].

4. Excitation Energies

In this section, RMCDHF/RCI excitation energies are compared with observations for a range of systems in order to illustrate the predictive power of highly accurate calculations. Generally, there are enough observations to validate computational methodologies and to distinguish between different approaches.

4.1. Energies for $2s^2 2p^n$, $2s2p^{n+1}$ and $2p^{n+2}$ States in the B-, C-, N-, O- and F-Like Sequences

Excitation energies and E1, M1, E2, M2 transition rates between $2s^2 2p^n$, $2s2p^{n+1}$ and $2p^{n+2}$ states of ions in the B-, C-, N-, O- and F-like sequences were calculated using the RMCDHF/RCI and SD-MR method [28–32]. The range of ions, as well as the details of the calculations are summarized in Table 1. Calculations of Landé g_J factors, hyperfine structures and isotope shifts were done separately for ions in the Be-, B-, C- and N-like sequences [33,34].

Table 1. Multireference (MR), active set, number of generated configuration state functions (CSFs) (N_{CSFs}) and the range of ions for the relativistic multiconfiguration Dirac-Hartree-Fock (RMCDHF) and relativistic configuration interaction (RCI) calculations of the boron-, carbon-, nitrogen-, oxygen- and fluorine-like sequences.

Configuration	MR for RMCDHF	MR for RCI	Active Set	N_{CSFs}
		boron-like, N III to Zn XXVI		
$1s^2 2s^2 2p$	$1s^2\{2s^2 2p, 2p^3\}$	$1s^2\{2s^2 2p, 2p^3, 2s2p3d, 2p3d^2\}$	$\{9s8p7d6f5g3h1i\}$	200 100
$1s^2 2p^3$	$1s^2\{2s^2 2p, 2p^3\}$	$1s^2\{2s^2 2p, 2p^3, 2s2p3d, 2p3d^2\}$	$\{9s8p7d6f5g3h1i\}$	360 100
$1s^2 2s2p^2$	$1s^2 2s2p^2$	$1s^2\{2s2p^2, 2p^2 3d, 2s^2 3d, 2s3d^2\}$	$\{9s8p7d6f5g3h1i\}$	300 100
		carbon-like, F IV to Ni XXIII		
$1s^2 2s^2 2p^2$	$1s^2\{2s^2 2p^2, 2p^4\}$	$1s^2\{2s^2 2p^2, 2p^4, 2s2p^2 3d, 2s^2 3d^2\}$	$\{8s7p6d5f4g2h\}$	340 100
$1s^2 2p^4$	$1s^2\{2s^2 2p^2, 2p^4\}$	$1s^2\{2s^2 2p^2, 2p^4, 2s2p^2 3d, 2s^2 3d^2\}$	$\{8s7p6d5f4g2h\}$	340 100
$1s^2 2s2p^3$	$1s^2 2s2p^3$	$1s^2\{2s2p^3, 2p^3 3d, 2s^2 2p3d, 2s2p3d^2\}$	$\{8s7p6d5f4g2h\}$	1 000 100
		nitrogen-like, F III to Kr XXX		
$1s^2 2s^2 2p^3$	$1s^2\{2s^2 2p^3, 2p^5\}$	$1s^2\{2s^2 2p^3, 2p^5, 2s2p^3 3d, 2s^2 2p3d^2\}$	$\{8s7p6d5f4g1h\}$	698 100
$1s^2 2p^5$	$1s^2\{2s^2 2p^3, 2p^5\}$	$1s^2\{2s^2 2p^3, 2p^5, 2s2p^3 3d, 2s^2 2p3d^2\}$	$\{8s7p6d5f4g1h\}$	382 100
$1s^2 2s2p^4$	$1s^2 2s2p^4$	$1s^2\{2s2p^4, 2p^4 3d, 2s^2 2p^2 3d, 2s2p^2 3d^2\}$	$\{8s7p6d5f4g1h\}$	680 100
		oxygen-like, F II to Kr XXIX		
$1s^2 2s^2 2p^4$	$1s^2\{2s^2 2p^4, 2p^6\}$	$1s^2\{2s^2 2p^4, 2p^6, 2s2p^4 3d\}$	$\{8s7p6d5f4g3h\}$	709 690
$1s^2 2p^6$	$1s^2\{2s^2 2p^4, 2p^6\}$	$1s^2\{2s^2 2p^4, 2p^6, 2s2p^4 3d\}$	$\{8s7p6d5f4g3h\}$	67 375
$1s^2 2s2p^5$	$1s^2 2s2p^5$	$1s^2\{2s2p^5, 2p^5 3d, 2s^2 2p^3 3d\}$	$\{8s7p6d5f4g3h\}$	702 892
		fluorine-like, Si VI to WLXVI		
$1s^2 2s^2 2p^5$	$1s^2 2s^2 2p^5$	$1s^2 2s^2 2p^5$	$\{8s7p6d5f4g3h2i\}$	73 000
$1s^2 2s2p^6$	$1s^2 2s2p^6$	$1s^2 2s2p^6$	$\{8s7p6d5f4g3h2i\}$	15 000

A trend for all atomic structure calculations, including RMCDHF/RCI, is that the accuracy of the excitation energies is, relatively speaking, lower for lowly charged ions and that the accuracy then increases as the effects of electron correlation diminish. For the highly charged ions, the situation is less clear. Often experimental excitation energies are associated with large uncertainties or missing altogether. The situation is illustrated in Tables 2 and 3 for the O-like sequence [31].

In Table 2, excitation energies in Ne III and Fe XIX from different calculations are compared with energies from observations. The most accurate calculations are the RMCDHF/RCI calculation [31] and the multireference second-order Möller-Plesset calculation (MRMP). For Ne III, the relative differences with observation for these two calculations are in the range of 0.2–0.4% (slightly worse for MRMP). For Fe XIX the relative errors go down by an order of magnitude, and now, the calculated energies are accurate enough to detect misidentifications or errors in observational data, but also to serve as a valuable tool for identifying new lines. The usefulness of computed energies is illustrated in Table 3 for Br XXVIII, where the RMCDHF/RCI and MRMP calculations clearly discriminate between

observed energies [35] and energies from semiempirical fits [36], being in better agreement with the latter. This suggests that there may be some calibration problems in relation to the observed energies [35].

Table 2. Excitation energies in cm^{-1} for O-like Ne and Fe from observations and different calculations. Relative errors in % for the calculated energies are shown in parenthesis. E_{obs} observation NIST [37], E_{RCI} energies from RMCDHF/RCI [31], E_{MRMP} energies from Möller-Plesset calculation (MRMP) [38], E_{MBPT} energies from many-body perturbation theory [39], E_{BP} energies from multiconfiguration Hartree-Fock-Breit-Pauli [19], E_{SS} energies from super structure [40], E_{MCDF} energies from RMCDHF [41] and E_{FAC} energies from RCI with the FAC code [42].

Ne III							
Level	***J***	E_{obs}	E_{RCI}	E_{MRMP}	E_{MBPT}	E_{BP}	E_{SS}
$2s^2 2p^4\ ^3P$	2	0	0 (0.00)	0 (0.00)	0 (0.00)	0 (0.00)	0 (0.00)
	1	643	645 (0.31)	638 (0.77)	645 (0.31)	628 (2.33)	744 (15.70)
	0	921	923 (0.21)	912 (0.97)	926 (0.54)	899 (2.38)	1 069 (16.06)
$2s^2 2p^4\ ^1D$	2	25 841	25 954 (0.43)	26 097 (0.99)	25 573 (1.03)	25 759 (0.31)	29 219 (13.07)
$2s^2 2p^4\ ^1S$	0	55 753	56 058 (0.54)	55 772 (0.03)	55 459 (0.52)	55 382 (0.66)	72 484 (30.00)
$2s2p^5\ ^3P^o$	2	204 290	204 608 (0.15)	204 718 (0.20)	200 686 (1.76)	204 635 (0.16)	215 348 (5.41)
	1	204 873	205 200 (0.15)	205 297 (0.20)	201 276 (1.75)	205 236 (0.17)	216 008 (5.43)
	0	205 194	205 603 (0.19)	205 617 (0.20)	201 598 (1.75)	205 539 (0.16)	216 367 (5.44)
$2s2p^5\ ^1P^o$	1	289 479	290 315 (0.28)	290 703 (0.42)	288 219 (0.43)	291 659 (0.75)	315 511 (8.99)
Fe XIX							
Level	***J***	E_{obs}	E_{RCI}	E_{MRMP}	E_{MBPT}	E_{MCDF}	E_{FAC}
$2s^2 2p^4\ ^3P$	2	0	0 (0.000)	0 (0.000)	0 (0.00)	0 (0.00)	0 (0.00)
	0	75 250	75 313 (0.083)	75 218 (0.042)	74 742 (0.67)	75 446 (0.26)	75 198 (0.06)
	1	89 441	89 434 (0.007)	89 251 (0.212)	87 559 (2.10)	88 791 (0.72)	88 821 (0.69)
$2s^2 2p^4\ ^1D$	2	168 852	168 985 (0.078)	168 792 (0.035)	167 881 (0.57)	170 847 (1.18)	170 578 (1.02)
$2s^2 2p^4\ ^1S$	0	325 140	325 417 (0.085)	324 949 (0.058)	321 124 (1.23)	326 536 (0.42)	325 421 (0.08)
$2s2p^5\ ^3P^o$	2	922 890	923 044 (0.016)	922 855 (0.003)	917 435 (0.59)	933 081 (1.10)	929 231 (0.68)
	1	984 740	984 920 (0.018)	984 791 (0.005)	978 242 (0.65)	995 006 (1.04)	991 246 (0.66)
	0	1030 020	1030 199 (0.017)	1029 992 (0.002)	1022 753 (0.70)	1039 692 (0.93)	1036 058 (0.58)
$2s2p^5\ ^1P^o$	1	1267 600	1268 093 (0.038)	1267 771 (0.013)	1258 927 (0.68)	1287 773 (1.59)	1282 914 (1.20)
$2p^6\ ^1S$	0	2134 180	2134 958 (0.036)	2132 810 (0.064)	2120 211 (0.65)	2175 645 (1.94)	2160 701 (1.24)

Table 3. Excitation energies in cm^{-1} for O-like Br. Comparison between calculations, observations and semiempirical estimates. E_{obs} observation NIST [37] with original data from Kelly [35], E_{SE} semiempirical fit [36] and E_{RCI} energies from RMCDHF/RCI [31], E_{MRMP} energies from MRMP [38]; ΔE_1, difference between calculated energies and E_{obs}; ΔE_2, difference between calculated energies and E_{SE}. The calculations support energies from the semiempirical fit.

Level	***J***	E_{obs}	E_{SE}	E_{RCI}	ΔE_1	ΔE_2	E_{MRMP}	ΔE_1	ΔE_2
$2s^2 2p^4\ ^3P$	2	0	0	0	0	0	0	0	0
	0	218 800	153 478	151 954	−66 846	−1524	15 2035	−66 765	−1443
	1	379 800	371 663	371 606	−8 194	−57	37 1858	−7 942	195
$2s^2 2p^4\ ^1D$	2	483 040	470 699	470 643	−12 397	−56	47 0804	−12 236	105
$2s^2 2p^4\ ^1S$	0	944 150	912 501	911 968	−32 182	-533	91 2282	−31 868	−219
$2s2p^5\ ^3P^o$	2		1 579 903	1 579 537		−366	1 580 945		1042
	1		1 755 028	1 755 196		168	1 756 684		1656
	0		1 986 274	1 985 784		−490	1 987 396		1122
$2s2p^5\ ^1P^o$	1		2 229 358	2 230 149		791	2 231 636		2278
$2p^6\ ^1S$	0		3 573 416	3 575 415		1999	3 579 486		6070

Summarizing the mean relative errors in the excitation energies for the $2s^2 2p^n$, $2s2p^{n+1}$ and $2p^{n+2}$ states of B-, C-, N-, O- and F-like Fe from RCI calculations [28–32], we have 0.022% for B-like, 0.022% for C-like, 0.050% for N-like, 0.042% for O-like and 0.011% for F-like Fe.

4.2. Energies of the $2s^2 2p^6$ and $2s^2 2p^5 3l$ States in the Ne-Like Sequence

The transitions connecting the $2s^2 2p^5 3l$, $l = 0, 1, 2$ configurations in Ne-like ions give rise to prominent lines in the spectra of many high temperature light sources. Some of these lines are considered for diagnostics of fusion plasmas. Excitation energies and E1, M1, E2, M2 transition rates between states of the above configurations in Ne-like Mg III and Kr XXVII sequences were calculated using the RMCDHF/RCI and SD-MR method [43]. The calculations were done based on expansions from SD substitutions from the $2s^2 2p^6$ and $2s^2 2p^5 3l$ configurations to active sets $\{7s6p5d4f3g2h1i\}$. The $1s^2$ was kept as a closed core. Some triple substitutions were allowed to capture higher order electron correlation effects. In Table 4, the RMCDHF/RCI excitation energies are displayed for Ca XI and Fe XVII. In the same table, the energies are compared with energies from NIST, as well as from MRMP calculations by Ishikawa et al. [44]. Again, the table illustrates the situation when it comes to experiments. For many ions, the excitation energies of the lower states are known from experiments. For other ions, such as Ca XI, energies are only known for a few states. The correlation model from the RMCDHF/RCI calculations predicts the excitation energies extremely well for all of the calculated ions. For Fe XVII, the relative differences with observations are around 0.005%. Calculated energies with this accuracy aid line identification in spectra and can be used to validate previous observations. As can be seen from the table, the RMCDHF/RCI and MRMP calculations both do very well, but the latter lose some of the accuracy at the neutral end of the sequence.

In Table 4, also the *LSJ* composition is shown for each state. There are many states that are heavily mixed, with terms of almost the same weight. In these cases, labelling becomes difficult, and for many ions in the sequence, there are states that have the same leading term. Labeling is a general problem that needs considerable attention [21].

4.3. Energies for Higher States in the B-, C-, N-, O-, F- and Ne-Like Sequences

In plasma modelling and diagnostics, it is important to provide atomic data for more than just the states of the lowest configurations. To meet this demand, the RMCDHF/RCI and SD-MR calculations for the B-, C-, N-, O-, F- and Ne-like sequences have been extended to hundreds of states in what we refer to as spectrum calculations [45–52]. The range of ions, the targeted configurations and the number of studied states for each sequence are summarized in Table 5. Calculations were done by parity, i.e., odd and even parity states were treated in separate sets of calculations. The targeted configurations define the MR, and the expansions were obtained by SD-MR substitutions from all subshells to increasing active sets of orbitals. In addition to excitation energies, E1, M1, E2 and M2 transition rates were calculated.

Spectrum calculations are challenging for different reasons. The active sets of orbitals often have to be large, since many states with different charge distributions should be represented. The large active sets lead to large CSF expansions, and typically, the number of CSFs are a few millions for each parity. Another challenge is to handle the labelling. With closely degenerate configurations, the states are often not pure, but need to be described by the leading *LSJ* composition. However, the *LSJ* composition depends on the details of the calculation and different calculation may lead to different compositions. Thus, it is not unusual that there are inconsistencies in labelling, making comparisons between different sets of calculations, as well as with observations difficult and time consuming.

Table 4. Excitation energies in cm^{-1} for Ne-like Ca and Fe from observations and different calculations. Relative errors in % for the calculated energies are shown in parenthesis. E_{obs} observation NIST [37], E_{RCI} energies from RMCDHF/RCI [43] and E_{MRMP} energies from MRMP [44].

Level	LSJ	Composition	E_{obs}	E_{RCI}	E_{MRMP}
			Ca XI		
$2p^6$	$^1S_0$	1.00	0	0	0
$2p^5 3s$	$^3P^o_2$	0.99		2 801 989	2 801 819
$2p^5 3s$	$^3P^o_1$	$0.62 + 0.38\ ^1P^o_1$	2 810 900	2 810 834 (0.0023)	2 810 588 (0.011)
$2p^5 3s$	$^3P^o_0$	0.99		2 831 800	2 831 670
$2p^5 3s$	$^1P^o_1$	$0.62 + 0.38\ ^3P^o_1$	2 839 900	2 839 662 (0.0084)	2 839 386 (0.018)
$2p^5 3p$	$^3S_1$	0.92		2 953 791	2 953 594
$2p^5 3p$	$^3D_2$	$0.68 + 0.24\ ^1D_2$		2 978 410	2 977 968
$2p^5 3p$	$^3D_3$	1.00		2 978 650	2 978 276
$2p^5 3p$	$^3D_1$	$0.43 + 0.36\ ^1P_1 + 0.20\ ^3P_1$		2 986 908	2 986 513
$2p^5 3p$	$^3P_2$	$0.65 + 0.34\ ^1D_2$		2 993 760	2 993 336
$2p^5 3p$	$^3D_1$	$0.54 + 0.40\ ^1P_1$		3 007 301	3 006 932
$2p^5 3p$	$^3P_0$	0.98		3 009 345	3 009 000
$2p^5 3p$	$^1D_2$	$0.41 + 0.31\ ^3D_2 + 0.27\ ^3P_2$		3 016 749	3 016 378
$2p^5 3p$	$^3P_1$	$0.68 + 0.24\ ^1P_1$		3 017 175	3 016 845
$2p^5 3p$	$^1S_0$	0.98		3 101 166	3 098 308
$2p^5 3d$	$^3P^o_0$	0.99		3 196 075	3 195 830
$2p^5 3d$	$^3P^o_1$	0.95	3 199 300	3 199 045 (0.0080)	3 198 902 (0.012)
$2p^5 3d$	$^3P^o_2$	0.85		3 205 278	3 205 169
$2p^5 3d$	$^3F^o_4$	1.00		3 208 351	3 208 165
$2p^5 3d$	$^3F^o_3$	$0.72 + 0.23\ ^1F^o_2$		3 212 392	3 212 144
$2p^5 3d$	$^3F^o_2$	$0.53 + 0.29\ ^1D^o_2 + 0.18\ ^3D^o_2$		3 219 655	3 219 428
$2p^5 3d$	$^3D^o_3$	$0.55 + 0.41\ ^1F^o_3$		3 224 394	3 224 078
$2p^5 3d$	$^3D^o_1$	0.89	3 239 700	3 239 502 (0.0061)	3 239 308 (0.012)
$2p^5 3d$	$^3F^o_2$	$0.47 + 0.38\ ^1D^o_2 + 0.14\ ^3D^o_2$		3 244 348	3 244 161
$2p^5 3d$	$^3D^o_2$	$0.58 + 0.27\ ^1D^o_2 + 0.14\ ^3P^o_2$		3 248 017	3 247 805
$2p^5 3d$	$^3D^o_3$	$0.40 + 0.35\ ^1F^o_3 + 0.24\ ^3F^o_3$		3 248 345	3 248 099
$2p^5 3d$	$^1P^o_1$	0.91	3 284 300	3 284 444 (0.0044)	3 283 473 (0.025)
			Fe XVII		
$2p^6$	$^1S_0$	1.00	0	0	0
$2p^5 3s$	$^3P^o_2$	1.00	5 849 490	5 849 108 (0.0065)	5 848 891 (0.0102)
$2p^5 3s$	$^1P^o_1$	$0.54 + 0.45\ ^3P_1$	5 864 760	5 864 469 (0.0049)	5 864 138 (0.0106)
$2p^5 3s$	$^3P^o_0$	1.00	5 951 478	5 951 003 (0.0079)	5 950 877 (0.0100)
$2p^5 3s$	$^3P^o_1$	$0.54 + 0.45\ ^1P_1$	5 961 022	5 960 633 (0.0065)	5 960 410 (0.0102)
$2p^5 3p$	$^3S_1$	$0.80 + 0.17\ ^3P_1$	6 093 568	6 093 573 (0.0000)	6 093 209 (0.0058)
$2p^5 3p$	$^3D_2$	$0.58 + 0.30\ ^1D_2 + 0.12\ ^3P_2$	6 121 756	6 121 769 (0.0002)	6 121 253 (0.0082)
$2p^5 3p$	$^3D_3$	1.00	6 134 815	6 134 794 (0.0003)	6 134 360 (0.0074)
$2p^5 3p$	$^1P_1$	$0.51 + 0.25\ ^3D_1 + 0.19\ ^3P_1$	6 143 897	6 143 898 (0.0000)	6 143 431 (0.0075)
$2p^5 3p$	$^3P_2$	$0.67 + 0.32\ ^1D_2$	6 158 540	6 158 481 (0.0009)	6 158 010 (0.0086)
$2p^5 3p$	$^3P_0$	0.94	6 202 620	6 202 542 (0.0012)	6 202 238 (0.0061)
$2p^5 3p$	$^3D_1$	$0.67 + 0.31\ ^1P_1$	6 219 266	6 219 185 (0.0013)	6 218 795 (0.0075)
$2p^5 3p$	$^3P_1$	$0.63 + 0.17\ ^1P_1 + 0.13\ ^3S_1$	6 245 490	6 245 346 (0.0023)	6 245 018 (0.0075)
$2p^5 3p$	$^3D_2$	$0.41 + 0.38\ ^1D_2 + 0.21\ ^3P_2$	6 248 530	6 248 390 (0.0022)	6 248 024 (0.0080)
$2p^5 3p$	$^1S_0$	0.93	6 353 356	6 353 605 (0.0039)	6 351 136 (0.0349)
$2p^5 3d$	$^3P^o_0$	0.99	6 464 095	6 463 913 (0.0028)	6 463 611 (0.0074)
$2p^5 3d$	$^3P^o_1$	0.91	6 471 233	6 471 519 (0.0044)	6 471 317 (0.0012)
$2p^5 3d$	$^3P^o_2$	$0.72 + 0.18\ ^3D^o_2$	6 486 440	6 486 166 (0.0042)	6 485 977 (0.0071)
$2p^5 3d$	$^3F^o_4$	1.00	6 487 000	6 486 745 (0.0039)	6 486 514 (0.0074)
$2p^5 3d$	$^3F^o_3$	$0.65 + 0.29\ ^1F^o_3$	6 492 924	6 492 689 (0.0036)	6 492 387 (0.0082)
$2p^5 3d$	$^1D^o_2$	$0.41 + 0.35\ ^3F^o_2 + 0.24\ ^3D^o_2$	6 506 808	6 506 561 (0.0037)	6 506 276 (0.0081)
$2p^5 3d$	$^3D^o_3$	$0.64 + 0.34\ ^1F^o_3$	6 515 479	6 515 276 (0.0031)	6 514 936 (0.0083)
$2p^5 3d$	$^3D^o_1$	$0.74 + 0.20\ ^1P^o_1$	6 552 221	6 552 697 (0.0072)	6 552 491 (0.0041)
$2p^5 3d$	$^3F^o_2$	$0.63 + 0.29\ ^1D^o_2$	6 594 617	6 594 260 (0.0054)	6 594 099 (0.0078)
$2p^5 3d$	$^3D^o_2$	$0.50 + 0.27\ ^3P^o_2 + 0.21\ ^1D^o_2$	6 601 210	6 600 855 (0.0053)	6 600 688 (0.0079)
$2p^5 3d$	$^1F^o_3$	$0.37 + 0.33\ ^3F^o_3 + 0.30\ ^3D^o_3$	6 605 469	6 605 078 (0.0059)	6 604 858 (0.0092)
$2p^5 3d$	$^1P^o_1$	$0.78 + 0.18\ ^3D^o_1$	6 660 894	6 661 101 (0.0031)	6 660 232 (0.0099)

Table 5. Sequence, ions and targeted configurations for the RMCDHF/RCI calculations. N is the number of studied states for each ion. In the table, $l = 0, 1, 2$, $l' = 0, 1, 2, 3$, $l'' = 0, \ldots, n-1$.

Sequence	Ions	Configurations	N	Ref.
B-like	Si, Ti-Cu	$2s^22p$, $2s2p^2$, $2p^3$, $2s^23l$, $2s2p3l$, $2p^23l$, $2s^24l'$, $2s2p4l'$, $2p^24l'$	291	[45]
B-like	Na	$2s^22p$, $2s2p^2$, $2p^3$, $2s^23l$, $2s2p3l$, $2p^23l$, $2s^24l'$, $2s2p4s$	133	[46]
C-like	Ar-Zn	$2s^22p^2$, $2s2p^3$, $2p^4$, $2s^22p3l$, $2s2p^23l$, $2p^33l$, $2s^22p4l$	262	[47]
N-like	Cr, Fe, Ni, Zn	$2s^22p^3$, $2s2p^4$, $2p^5$, $2s^22p^23l$, $2s2p^33l$, $2p^43l$	272	[48]
N-like	Ar-Zn	$2s^22p^3$, $2s2p^4$, $2p^5$, $2s^22p^23l$, $2s2p^33l$, $2p^43l$, $2s^22p^24l'$	359	[49]
O-like	Cr-Zn	$2s^22p^4$, $2s2p^5$, $2p^6$, $2s^22p^33l$, $2s2p^43l$	200	[50]
F-like	Cr-Zn	$2s^22p^5$, $2s2p^6$, $2s^22p^43l$, $2s2p^53l$, $2p^63l$, $2s^22p^44l'$	200	[51]
Ne-like	Cr-Kr	$2s^22p^6$, $2s2p^63l$, $2s^22p^54l$, $2s2p^64l$, $2s^22p^55l''$, $2s^22p^56l''$	201	[52]

For many ions, excitation energies for lower lying states are known from observations. Going higher, comparatively less data are available, and these are often associated with large uncertainties. The situation is well illustrated for C-like Fe, and in Table 6, the RMCDHF/RCI excitation energies by Ekman et al. [47] are compared with observations. Due to near degeneracies, many states have the same leading LSJ term. In these cases, labelling can be done either by giving the leading terms in the composition or, more simply, introducing an additional index A and B to separate the states. For the 20 first states belonging to the $n = 2$ configurations, observations are available from the NIST [37] and CHIANTI databases [3,4]. There is an agreement between the RMCDHF/RCI and relativistic many body calculations (RMBPT) by Gu [53] and observations at the 0.028–0.032% level (slightly worse for RMBPT). The RCI calculation using the Flexible Atomic Code (FAC) [42] is less accurate. For the higher lying states, experimental data are sparse. In many cases, there is excellent agreement between observations and calculations also for these states, but in some cases, there are obvious disagreements. For State Number 36, the excitation energy from NIST and CHIANTI disagree, and the calculations by Ekman et al. and Gu support the energy from the CHIANTI database. For State 54, all calculations agree, but differ markedly from the energies given by NIST and CHIANTI.

Table 6. Energies in cm^{-1} for levels in Fe XXI. E_{RCI} energies from RMCDHF/RCI calculations [47], E_{RMBPT} energies from RMBPT [53], E_{FAC} energies from RCI calculations with FAC [42], E_{NIST} NIST recommended values [37] and E_{CHI} observed energies from the CHIANTI database [3,4].

No.	Level	E_{RCI}	E_{RMBPT}	E_{FAC}	E_{NIST}	E_{CHI}
1	$2s^22p^2\ ^3P_0$	0	0	0	0	0
2	$2s^22p^2\ ^3P_1$	73 864	73 867	73 041	73 851	73 851
3	$2s^22p^2\ ^3P_2$	117 417	117 372	117 146	117 354	117 367
4	$2s^22p^2\ ^1D_2$	244 751	244 581	245 710	244 561	244 568
5	$2s^22p^2\ ^1S_0$	372 137	372 261	373 060	371 980	371 744
6	$2s2p^3\ ^5S_2$	486 584	487 683	479 658	486 950	486 991
7	$2s2p^3\ ^3D_1$	776 775	777 005	779 724	776 690	776 685
8	$2s2p^3\ ^3D_2$	777 404	777 655	779 963	777 340	777 367
9	$2s2p^3\ ^3D_3$	803 618	803 869	805 768	803 540	803 553
10	$2s2p^3\ ^3P_0$	916 444	916 773	920 272	916 330	916 333
11	$2s2p^3\ ^3P_1$	925 074	925 408	928 822	924 920	924 920
12	$2s2p^3\ ^3P_2$	942 621	942 986	946 135	942 430	942 364
13	$2s2p^3\ ^3S_1$	1 096 019	1 095 820	1 105 578	1 095 670	1 095 679
14	$2s2p^3\ ^1D_2$	1 127 672	1 127 460	1 137 533	1 127 240	1 127 250
15	$2s2p^3\ ^1P_1$	1 261 577	1 261 240	1 272 627	1 261 140	1 260 902
16	$2p^4\ ^3P_2$	1 646 437	1 646 467	1 657 411	1 646 300	1 646 409
17	$2p^4\ ^3P_0$	1 735 823	1 735 813	1 747 301	1 735 700	1 735 715
18	$2p^4\ ^3P_1$	1 740 623	1 740 707	1 750 848	1 740 500	1 740 453
19	$2p^4\ ^1D_2$	1 817 786	1 817 362	1 832 102	1 817 100	1 817 041
20	$2p^4\ ^1S_0$	2 048 512	2 047 850	2 066 463	2 048 200	2 048 056
21	$2s^22p3s\ ^3P_0$	7 663 283	7 664 054	7 654 119		
22	$2s^22p3s\ ^3P_1$	7 671 971	7 672 703	7 663 398		7 661 883

Table 6. *Cont.*

No.	Level	E_{RCI}	E_{RMBPT}	E_{FAC}	E_{NIST}	E_{CHI}
23	$2s^2 2p3s\ ^3P_2$	7 780 298	7 781 147	7 770 895		
24	$2s^2 2p3s\ ^1P_1$	7 803 764	7 804 419	7 796 397		
25	$2s^2 2p3p\ ^3D_1$	7 841 903	7 842 922	7 834 847		
26	$2s^2 2p3p\ ^3P_1 : A$	7 898 154	7 898 974	7 891 978		
27	$2s^2 2p3p\ ^3D_2$	7 901 553	7 902 378	7 895 497		
28	$2s^2 2p3p\ ^3P_0$	7 914 849	7 915 811	7 909 434		7 915 463
29	$2s^2 2p3p\ ^3P_1 : B$	7 983 446	7 984 350	7 977 011		
30	$2s^2 2p3p\ ^3D_3$	7 994 588	7 995 388	7 987 318		
31	$2s^2 2p3p\ ^3S_1$	8 004 987	8 005 793	7 998 341		
32	$2s^2 2p3p\ ^3P_2$	8 007 326	8 008 319	8 002 052		
33	$2s^2 2p3p\ ^1D_2$	8 068 537	8 069 071	8 065 382		
34	$2s^2 2p3d\ ^3F_2$	8 078 540	8 079 119	8 072 911		8 074 160
35	$2s2p^2(4P)3s\ ^5P_1$	8 080 551	8 082 001	8 070 805		
36	$2s^2 2p3d\ ^3F_3$	8 116 048	8 116 480	8 111 336	8 101 400	8 118 008
37	$2s^2 2p3d\ ^3P_2 : A$	8 121 922	8 122 529	8 118 025		8 124 085
38	$2s^2 2p3p\ ^1S_0$	8 128 645	8 129 396	8 126 192		8 143 710
39	$2s2p^2(4P)3s\ ^5P_2$	8 131 973	8 133 460	8 121 258		
40	$2s^2 2p3d\ ^3D_1$	8 139 290	8 140 735	8 135 992	8 140 000	8 141 785
41	$2s2p^2(4P)3s\ ^5P_3$	8 181 331	8 182 599	8 170 876		
42	$2s2p^2(4P)3s\ ^3P_0$	8 182 172	8 182 844	8 179 292		8 180 254
43	$2s^2 2p3d\ ^3F_4$	8 202 073	8 202 670	8 195 771		
44	$2s^2 2p3d\ ^1D_2$	8 208 705	8 209 597	8 204 329		
45	$2s2p^2(4P)3s\ ^3P_1$	8 222 156	8 222 948	8 217 390		
46	$2s^2 2p3d\ ^3D_3$	8 230 918	8 231 868	8 227 144	(8 195 000)	8 229 642
47	$2s^2 2p3d\ ^3P_2 : B$	8 245 453	8 246 428	8 241 436	8 230 900	8 229 642
48	$2s^2 2p3d\ ^3P_1$	8 245 737	8 247 075	8 241 557		
49	$2s^2 2p3d\ ^3P_0$	8 247 732	8 249 164	8 243 033		
50	$2s2p^2(4P)3p\ ^5D_0$	8 267 963	8 269 220	8 259 742		
51	$2s2p^2(4P)3p\ ^5D_1$	8 270 558	8 272 088	8 262 373		
52	$2s2p^2(4P)3s\ ^3P_2$	8 274 704	8 275 427	8 270 235		
53	$2s^2 2p3d\ ^1F_3$	8 300 618	8 301 128	8 301 379	8 313 600	
54	$2s^2 2p3d\ ^1P_1$	8 303 730	8 307 428	8 305 376	8 293 900	8 293 791
55	$2s2p^2(4P)3p\ ^5D_2$	8 305 917	8 309 162	8 297 457		
56	$2s2p^2(4P)3p\ ^3S_1$	8 312 499	8 309 359	8 300 070		
57	$2s2p^2(4P)3p\ ^5P_1$	8 349 456	8 350 857	8 342 324		8 350 731
58	$2s2p^2(4P)3p\ ^5D_3$	8 351 775	8 353 277	8 342 522		
59	$2s2p^2(4P)3p\ ^5P_2$	8 352 117	8 353 731	8 343 801		
60	$2s2p^2(4P)3p\ ^3D_1$	8 379 967	8 380 890	8 373 689		8 376 741
61	$2s2p^2(4P)3p\ ^5P_3$	8 388 634	8 390 292	8 380 281		
62	$2s2p^2(4P)3p\ ^5D_4$	8 399 557	8 401 039	8 390 478		
63	$2s2p^2(4P)3p\ ^3D_2$	8 410 077	8 411 182	8 404 386		
64	$2s2p^2(2D)3s\ ^3D_1$	8 420 588	8 421 426	8 420 569		
65	$2s2p^2(2D)3s\ ^3D_2$	8 428 405	8 429 248	8 428 172		
66	$2s2p^2(2D)3s\ ^3D_3$	8 440 926	8 441 758	8 437 725		
67	$2s2p^2(4P)3p\ ^3P_0$	8 442 813	8 443 776	8 438 241		
68	$2s2p^2(4P)3p\ ^5S_2$	8 443 646	8 445 037	8 440 027		
69	$2s2p^2(4P)3p\ ^3D_3$	8 462 365	8 463 510	8 456 502		
70	$2s2p^2(4P)3p\ ^3P_1$	8 467 690	8 468 680	8 462 413		
71	$2s2p^2(4P)3p\ ^3P_2$	8 470 871	8 471 913	8 466 158		
72	$2s2p^2(4P)3d\ ^5F_1$	8 480 620	8 481 735	8 471 575		
73	$2s2p^2(4P)3d\ ^5F_2$	8 488 782	8 489 971	8 479 898		8 486 331
74	$2s2p^2(2D)3s\ ^1D_2$	8 496 990	8 497 512	8 498 660		
75	$2s2p^2(4P)3d\ ^5F_3 : A$	8 506 111	8 507 343	8 497 311		8 511 385
76	$2s2p^2(4P)3d\ ^5F_4$	8 544 575	8 545 928	8 534 831		
77	$2s2p^2(2P)3s\ ^3P_1$	8 545 485	8 546 507	8 544 603		
78	$2s2p^2(2P)3s\ ^3P_0$	8 553 885	8 554 716	8 545 420		
79	$2s2p^2(4P)3d\ ^5D_0$	8 554 798	8 555 918	8 546 365		
80	$2s2p^2(4P)3d\ ^5D_1$	8 555 297	8 556 534	8 547 553		
81	$2s2p^2(4P)3d\ ^5D_2$	8 555 491	8 556 850	8 558 611		
82	$2s2p^2(4P)3d\ ^5F_3 : B$	8 561 662	8 562 969	8 552 789		8 564 535
83	$2s2p^2(4P)3d\ ^3P_2$	8 581 274	8 582 755	8 576 965		8 575 780

Table 6. *Cont.*

No.	Level	E_{RCI}	E_{RMBPT}	E_{FAC}	E_{NIST}	E_{CHI}
84	$2s2p^2(4P)3d\ ^5F_5$	8 586 636	8 588 014	8 577 151		
85	$2s2p^2(4P)3d\ ^5D_4$	8 597 735	8 599 106	8 588 388		
86	$2s2p^2(2D)3p\ ^3F_2$	8 606 110	8 606 654	8 607 148		8 605 427
87	$2s2p^2(4P)3d\ ^3F_2$	8 611 432	8 611 843	8 608 283		
88	$2s2p^2(4P)3d\ ^5P_3$	8 619 312	8 620 847	8 611 148		
			⋮			
228	$2p^3(^2P)3d\ ^3F_4$	9 735 480	9 736 111	9 746 771		
229	$2p^3(^2P)3d\ ^3P_1$	9 740 645	9 742 719	9 754 847		
230	$2p^3(^2P)3d\ ^3P_0$	9 748 184	9 749 774	9 758 859		
231	$2p^3(^2P)3d\ ^3P_2 : B$	9 757 890	9 758 107	9 770 963		
232	$2p^3(^2P)3d\ ^3D_1$	9 765 663	9 766 056	9 781 499		
233	$2p^3(^2P)3d\ ^3D_3$	9 780 738	9 781 044	9 794 389		
234	$2p^3(^2P)3d\ ^1F_3$	9 800 368	9 800 742	9 819 206		
235	$2p^3(^2P)3d\ ^3D_2$	9 800 852	9 801 738	9 819 939		
236	$2p^3(^2P)3d\ ^1P_1$	9 879 471	9 879 655	9 902 175		
237	$2s^22p4s\ ^3P_0$	10 368 077		10 362 393		
238	$2s^22p4s\ ^3P_1$	10 371 121		10 365 585	10 380 000	
239	$2s^22p4p\ ^3D_1$	10 442 616		10 437 633		
240	$2s^22p4p\ ^3P_1$	10 466 102		10 460 676		
241	$2s^22p4p\ ^3D_2$	10 468 322		10 462 978		
242	$2s^22p4p\ ^3P_0$	10 470 990		10 465 993		
243	$2s^22p4s\ ^3P_2$	10 485 597		10 479 693		
244	$2s^22p4s\ ^1P_1$	10 492 966		10 487 317		
245	$2s^22p4d\ ^3F_2$	10 532 099		10 526 459		
246	$2s^22p4d\ ^3P_2 : A$	10 548 542		10 542 323	(10 547 000)	10 547 249
247	$2s^22p4d\ ^3F_3$	10 549 480		10 543 488	10 548 000	10 548 160
248	$2s^22p4d\ ^3D_1$	10 554 447		10 548 345	10 553 000	10 553 955
249	$2s^22p4p\ ^1P_1$	10 568 810		10 563 327		
250	$2s^22p4p\ ^3D_3$	10 574 912		10 569 412	10 664 000	
251	$2s^22p4p\ ^3P_2$	10 575 111		10 569 433		
252	$2s^22p4p\ ^3S_1$	10 578 203		10 572 657		
253	$2s^22p4p\ ^1D_2$	10 597 862				
254	$2s^22p4p\ ^1S_0$	10 619 563				
255	$2s^22p4d\ ^3F_4$	10 652 979				
256	$2s^22p4d\ ^1D_2$	10 653 631			10 675 000	
257	$2s^22p4d\ ^3D_3$	10 660 593				
258	$2s^22p4d\ ^3P_2 : B$	10 666 807				
259	$2s^22p4d\ ^3P_1$	10 666 946			10 688 000	
260	$2s^22p4d\ ^3P_0$	10 667 948				
261	$2s^22p4d\ ^1F_3$	10 683 984			10 681 000	
262	$2s^22p4d\ ^1P_1$	10 687 400				

One should note the excellent agreement between the energies from RMCDHF/RCI and RMBPT, the mean difference being less than 0.013%. Although the energies are in very good agreement, there seems to be a small systematic shift for the higher states, as depicted in Figure 1. The reason for this shift is not known, and further research is needed to shed light on this. To further access the accuracy of the excitation energies, calculations for the N-, O-, F- and Ne-like sequences [49–52] were done using both the RMCDHF/RCI and RMBPT methods. Cross-validations show that the mean energy differences for N-like, O-like, F-like and Ne-like Fe are 0.023%, 0.011%, 0.01% and 0.029%, respectively. The energy differences increase for the ions closer to the neutral end, where the RMBPT method is less efficient in capturing correlation effects.

Obviously, calculations with high accuracy that also give the leading *LSJ* compositions are indispensable tools for analysing astrophysical observations.

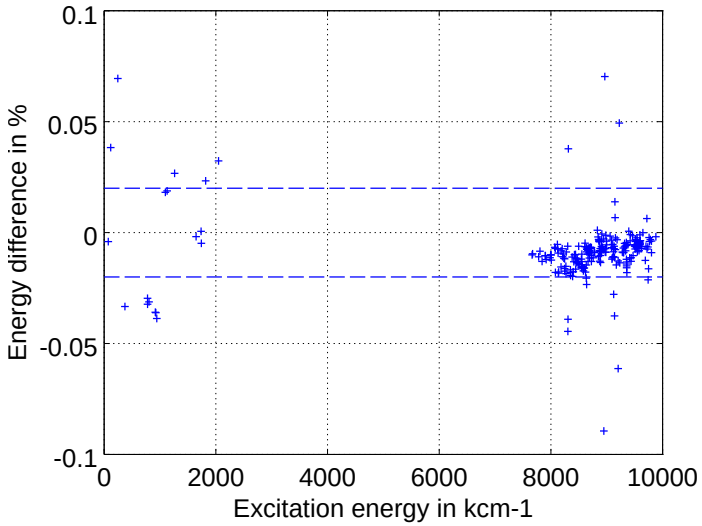

Figure 1. Difference between RMCDHF/RCI and MBPT excitation energies in percent for C-like Fe as a function of the excitation energy in kcm^{-1}. The dashed lines show the 0.02 % levels.

4.4. Energies for Higher Lying States in the Mg-, Al- and Si-Like Sequences

For larger atomic systems, one needs to think in terms of a core and a number of valence electrons. In many calculations, only valence-valence (VV) correlation is included. More accurate results are obtained when accounting for the interactions with the core through the inclusion of core-valence correlation (VV + CV). The final step is to include core-core correlation (VV + CV + CC). The situation has been analysed by Gustafsson et al. [12] for $3l3l'$, $3l4l'$, $3s5l$ states in Mg-like Fe where $1s^2 2s^2 2p^6$ is taken as the core. The results of the analysis can be inferred from Figure 2 that shows the difference between the computed excitation energies and the observed energies from the NIST database as a function of the excitation energies for the three computational models: VV, VV + CV and VV + CV + CC.

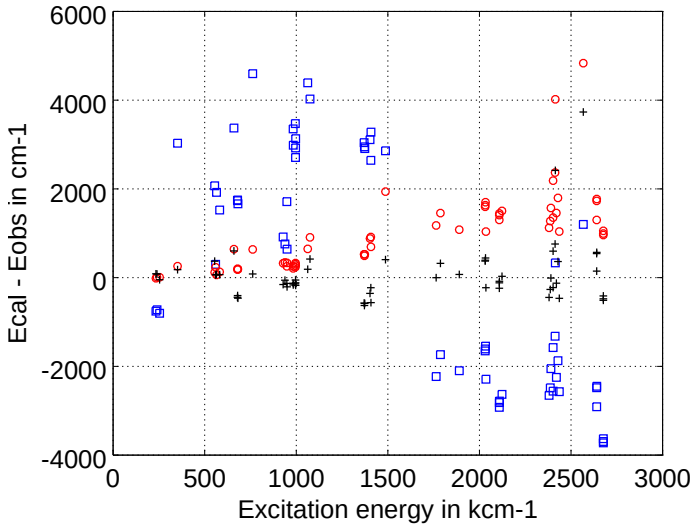

Figure 2. Difference between observed and RMCDHF/RCI excitation energies in cm^{-1} for Mg-like Fe [12] as a function of the excitation energy in kcm^{-1}. valence-valence (VV) (blue squares), VV + core-valence (CV) (red circles) and VV + CV + CC (black+).

From the figure, we see that the differences between the RMCDHF/RCI energies and observed energies are quite large, of the order of several thousand cm^{-1}, for the VV model. For many of

the low lying states, calculated energies are too high, whereas for the more highly lying states, calculated energies are too low. Adding core-valence correlation (VV + CV) substantially improves the calculated energies. To explain the difference in behaviour, as shown in the figure, between the low lying states and the more high lying states when core-valence correlation is added, we note that core-valence correlation is a combination of core polarization, an electrostatic long range rearrangement and an electron-electron cusp correcting effect [7,8]. The cusp correcting effect lowers all energies with an amount that depends on the overlap of the valence electron charge distribution and the core. The charge distributions of the low lying states from the $3l3l'$ configurations are to a larger extent overlapping the core region compared to the charge distributions from the higher states of the $3l4l'$ and $3l5l'$ configurations, leading to a more pronounced energy lowering for the former states. The core polarization, in turn, lowers all energies except the $3s^2\ ^1S_0$ ground state for which the valence electron charge density is spherically symmetric. In total, these two effects explain the observed behaviour. Whereas the low lying states are now in very good agreement with observations, the high lying states are still a little high compared to observations. The effect of the core-core correlation (VV + CV + CC) is small for the low lying states, but brings down the more highly states that are now in perfect agreement with observations.

The increased accuracy comes with a price. For an orbital set $\{8s7p6d5f4g3h2i\}$, the valence-valence (VV) expansions sizes are less than 3000 CSFs for each parity. Including the core-valence correlation (VV + CV) increases the expansions sizes to around 650,000 CSFs for each parity. Finally, including also core-core (VV + CV + CC) make the expansion sizes grow to around 6,000,000 CSFs for each parity. For these large expansions, it becomes necessary to use a zero- and first-order partition of the CSFs and include part of the interactions perturbatively as described in Section 2.3.

Based on the valence-valence and core-valence model (VV + CV), RMCDHF/RCI and SD-MR calculations have been done for the Mg-, Al- and Si-like sequences [54–56]. The range of ions, the targeted configurations and the number of studied states for each sequence are summarized in Table 7. Calculations were done by parity, i.e., odd and even parity states were treated in separate sets of calculations. The targeted configurations define the MR, and the expansions were obtained by SD-MR substitutions to increasing active sets of orbitals with the restriction that only one substitution is allowed from the $2s^22p^6$ core. $1s^2$ is treated as an inactive core and is always closed.

Table 7. Sequence, ions and targeted configurations for the calculations. N is the number of studied states for each ion. In the table, $l = 0, \ldots, n-1$, $l' = 0, \ldots, n-1$.

Sequence	Ions	Configurations	N	Ref.
Mg-like	Ca-As, Kr	$3l3l'$, $3l4l'$, $3s5l$	146	[54]
Al-like	Ti-Kr, Xe, W	$3s^2\{3l;4l;5l\}$, $3p^2\{3d;4l\}$, $3s\{3p^2;3d^2\}$, $3s\{3p3d;3p4l;3p5s;3d4l'\}$, $3p3d^2$, $3p^3$, $3d^3$	360	[55]
Si-like	Ti-Ge, Sr, Zr, Mo	$3s^23p^2$, $3s3p^3$, $3s^23p3d$	27	[56]

To illustrate the accuracy of the RMCDHF/RCI calculation accounting for valence-valence and core-valence effects, we look at Si-like Fe [56]. In Table 8, the computed excitation RMCDHF/RCI energies are compared with observed energies from Del Zanna [57], as well as with energies by Vilkas and Ishikawa [58] using the MRMP method. The mean deviation is 0.076% for RMCDHF/RCI and only 0.034% for MRMP. The expansions for the even and odd states contained 1,500,000 and 4,500,000 CSFs, respectively.

The mean energy deviations for Mg-like, Al-like and Si-like iron from RMCDHF/RCI calculation accounting for valence-valence and core-valence effects are 0.051%, 0.039% and 0.076%, respectively. To improve the energies for the RMCDHF/RCI calculations, core-core correlation effects can be included as perturbative corrections, and work is in progress to develop tractable computational methods. For systems with five and more valence electrons, the expansions grow rapidly, and it

may be necessary to start with valence-valence correlation and include core-valence effects as perturbative corrections.

Table 8. Comparison of calculated and observed excitation energies in cm^{-1}. E_{RCI} RMCDHF/RCI energies from [56], E_{MRMP} MRMP energies from [58] and E_{DZ} observed energies from [57]. Relative errors in % for the calculated energies are shown in parenthesis.

Fe XIII			
Level	E_{RCI}	E_{MRMP}	E_{DZ}
$3s^2\,3p^2\,{}^3P_0$	0	0	0
$3s^2\,3p^2\,{}^3P_1$	9281 (0.237)	9295 (0.086)	9303.1
$3s^2\,3p^2\,{}^3P_2$	18553 (0.048)	18576 (0.075)	18561.7
$3s^2\,3p^2\,{}^1D_2$	48236 (0.344)	47985 (1.077)	48069.7
$3s^2\,3p^2\,{}^1S_0$	91839 (0.357)	91508 (0.003)	91511.0
$3s\,3p^3\,{}^5S^o_2$	214152 (0.220)	214540 (0.039)	214624.0
$3s\,3p^3\,{}^3D^o_1$	287123 (0.028)	287199 (0.002)	287205.0
$3s\,3p^3\,{}^3D^o_2$	287270 (0.029)	287348 (0.002)	287356.0
$3s\,3p^3\,{}^3D^o_3$	290095 (0.029)	290179 (0.000)	290180.0
$3s\,3p^3\,{}^3P^o_0$	328974 (0.014)	328980 (0.016)	328927.0
$3s\,3p^3\,{}^3P^o_1$	329689 (0.015)	329702 (0.019)	329637.0
$3s\,3p^3\,{}^3P^o_2$	330323 (0.012)	330334 (0.015)	330282.0
$3s\,3p^3\,{}^1D^o_2$	362482 (0.020)	362416 (0.002)	362407.0
$3s\,3p^3\,{}^3S^o_1$	415577 (0.027)	415519 (0.013)	415462.0
$3s^2\,3p\,3d\,{}^3F^o_2$	430277 (0.035)	430129 (0.001)	430124.0
$3s^2\,3p\,3d\,{}^3F^o_3$	437064 (0.033)	436905 (0.003)	436919.0
$3s\,3p^3\,{}^1P^o_1$	438365 (0.063)	438005 (0.018)	438086.0
$3s^2\,3p\,3d\,{}^3F^o_4$	447134 (0.029)	446959 (0.009)	447001.0
$3s^2\,3p\,3d\,{}^3P^o_2$	486542 (0.037)	486403 (0.009)	486358.0
$3s^2\,3p\,3d\,{}^3P^o_1$	495102 (0.032)	495242 (0.060)	494942.0
$3s^2\,3p\,3d\,{}^1D^o_2$	499060 (0.038)	498925 (0.011)	498870.0
$3s^2\,3p\,3d\,{}^3P^o_0$	501676 (0.032)	501667 (0.030)	501514.0
$3s^2\,3p\,3d\,{}^3D^o_1$	506661 (0.030)	506681 (0.034)	506505.0
$3s^2\,3p\,3d\,{}^3D^o_3$	509303 (0.024)	509479 (0.059)	509176.0
$3s^2\,3p\,3d\,{}^3D^o_2$	509394 (0.028)	509441 (0.037)	509250.0
$3s^2\,3p\,3d\,{}^1F^o_3$	557432 (0.093)	557303 (0.070)	556911.0
$3s^2\,3p\,3d\,{}^1P^o_1$	571376 (0.110)	571187 (0.077)	570743.0

5. Transition Probabilities

Whereas there are enough observations to validate calculated excitation energies, the situation is very different for transition rates. For highly charged ions, there are few experimental methods available to determine transition rates. Lifetimes for long-lived states of the ground configuration or the lowest excited configurations have been determined in accurate storage-ring and trapping experiments (see for example, the review by Träbert [59]) and are used for benchmarking. Lifetimes for a large range of short-lived states have been determined using beam-foil spectroscopy [60]. However, even if these beam-foil data are very valuable, they are in general not accurate enough to discriminate between different computational approaches. In addition, lifetimes are dominated by the strong decay channels down to the lower configurations, and the lack of experimental transition rates, including weak transitions, between states of the excited configurations is of a major concern.

5.1. Internal Validation and Uncertainty Estimates

Due to the almost complete lack of experimental transition rates for highly charged ions, internal validation becomes important. For RMCDHF/RCI calculations, the convergence of the transition rates should be monitored as the active set is increased. Then, based on the same logic, the convergence of the transition rates should be monitored as the more involved correlation models are used, e.g., VV, VV + CV and VV + CV + CC. Considering the fact that there often are tens of thousands of transitions for extended spectrum calculations, this validation method is impractical,

and only smaller numbers of selected transitions can be monitored. Another internal validation method is based on the accuracy of the transition energy and the agreement between the computed line strength S in the length and velocity gauge. Along these lines, Froese-Fischer [61] has suggested that the uncertainties $\delta A'$ of the calculated transition rates for LS allowed transitions can be estimated according to:

$$\delta A' = (\delta E + \delta S)A', \tag{9}$$

where A' is the energy-scaled transition rate computed from the observed transition energy (E_{obs}), $\delta E = |E_{calc} - E_{obs}|/E_{obs}$ is the relative error in the transition energy and $\delta S = |S_{len} - S_{vel}|/\max(S_{len}, S_{vel})$ is the relative discrepancy between the length and velocity forms of the line strengths. In cases where the transition energies are not known, the expression reduces to:

$$\delta A = (\delta S)A. \tag{10}$$

Based on a statistical analysis of large datasets of accurate E1 transition rates from many independent calculations, Ekman et al. [62] found that the estimated errors from Equation (10) are correlated with and very close to the presumed actual errors. A validation of the method extended to intercombination lines reveals a smaller correlation in the statistical analysis and suggests that the uncertainty estimate in this case should only be used if averaging over a larger sample. The analysis further confirms the well-known fact that the uncertainty is large for weaker transitions, the general explanation being cancellations between the contributions to the matrix elements from different pairs of CSFs [63] or cancellations in the integrands of the transition integrals.

5.2. Transition Rates for the B- to Si-Like Sequences

The RMCDHF/RCI and SD-MR method has been used to compute tens of thousands of E1, M1, E2, M2 transitions rates for the B- to Si-like sequences [28–32,43,45–52,54–56]. The E1 and E2 rates are internally validated by giving $\delta A/A$ along with A. The results for C-like Fe [29], shown in Table 9, illustrate the typical uncertainties. The table displays computed transition energies along with relative uncertainties obtained by comparing with observations from NIST. The uncertainties for the transition energies are all well below 1%, and many of them are around 0.1%, which is highly satisfactory. The transition rates in the length form are given together with the uncertainty estimate $\delta A/A$. The uncertainties for the transition rates are a few percent or less for the strong transitions, but go up to around 20% for some of the weak intercombination transitions. To further shed light on the situation, we compare the RMCDHF/RCI rates for Ne-like S [43] with rates from accurate MCHF-BP calculations [19] and with CI calculations using CIV3 [64] in Table 10. From the table, we see that there is in general a very good agreement between the rates from the different calculations. It is clear that the largest differences are for the weak transitions.

Table 9. Transition energies in cm^{-1} and E1 rates A in s^{-1} in the length gauge for Fe XXI from RMCDHF/RCI calculations [29]. Relative errors in % for the calculated transition energies and rates are shown in parenthesis. For the transition energies, the relative errors were obtained by comparison with observations from NIST. For the transition rates, the relative errors are estimated from Equation (10).

Upper	Lower	ΔE_{calc}	A
		Fe XXI	
$2s2p^3\ ^3D^o_1$	$2s^22p^2\ ^3P_0$	776750 (0.049)	1.156E+10 (0.00)
$2s2p^3\ ^3P^o_1$	$2s^22p^2\ ^3P_0$	925023 (0.120)	4.213E+09 (0.07)
$2s2p^3\ ^3S^o_1$	$2s^22p^2\ ^3P_0$	1096012 (0.089)	9.460E+09 (0.16)
$2s2p^3\ ^1P^o_1$	$2s^22p^2\ ^3P_0$	1261529 (0.205)	2.850E+07 (1.82)
$2s2p^3\ ^5S^o_2$	$2s^22p^2\ ^3P_1$	412701 (0.293)	3.597E+07 (8.72)

Table 9. *Cont.*

Upper	Lower	ΔE_{calc}	A
$2s2p^3\ ^3D^o_1$	$2s^22p^2\ ^3P_1$	702930 (0.049)	7.606E+08 (1.64)
$2s2p^3\ ^3D^o_2$	$2s^22p^2\ ^3P_1$	703550 (0.048)	9.240E+09 (0.66)
$2s2p^3\ ^3P^o_0$	$2s^22p^2\ ^3P_1$	842581 (0.122)	2.200E+10 (0.31)
$2s2p^3\ ^3P^o_1$	$2s^22p^2\ ^3P_1$	851203 (0.119)	1.602E+10 (0.12)
$2s2p^3\ ^3P^o_2$	$2s^22p^2\ ^3P_1$	868735 (0.120)	3.820E+08 (1.85)
$2s2p^3\ ^3S^o_1$	$2s^22p^2\ ^3P_1$	1022191 (0.133)	2.533E+10 (0.11)
$2s2p^3\ ^1D^o_2$	$2s^22p^2\ ^3P_1$	1053811 (0.089)	3.907E+08 (1.68)
$2s2p^3\ ^1P^o_1$	$2s^22p^2\ ^3P_1$	1187709 (0.205)	4.909E+09 (0.34)
$2s2p^3\ ^5S^o_2$	$2s^22p^2\ ^3P_2$	369157 (0.293)	3.272E+07 (11.61)
$2s2p^3\ ^3D^o_1$	$2s^22p^2\ ^3P_2$	659387 (0.050)	8.335E+07 (6.39)
$2s2p^3\ ^3D^o_2$	$2s^22p^2\ ^3P_2$	660006 (0.050)	4.535E+06 (22.51)
$2s2p^3\ ^3D^o_3$	$2s^22p^2\ ^3P_2$	686197 (0.050)	6.105E+09 (0.80)
$2s2p^3\ ^3P^o_1$	$2s^22p^2\ ^3P_2$	807659 (0.120)	2.681E+09 (1.30)
$2s2p^3\ ^3P^o_2$	$2s^22p^2\ ^3P_2$	825192 (0.121)	2.038E+10 (0.04)
$2s2p^3\ ^3S^o_1$	$2s^22p^2\ ^3P_2$	978647 (0.134)	6.104E+10 (0.24)
$2s2p^3\ ^1D^o_2$	$2s^22p^2\ ^3P_2$	1010267 (0.090)	8.020E+09 (0.39)
$2s2p^3\ ^1P^o_1$	$2s^22p^2\ ^3P_2$	1144165 (0.206)	2.491E+08 (0.16)
$2s2p^3\ ^5S^o_2$	$2s^22p^2\ ^1D_2$	241853 (0.714)	1.307E+06 (19.51)
$2s2p^3\ ^3D^o_1$	$2s^22p^2\ ^1D_2$	532083 (0.048)	1.808E+08 (6.63)
$2s2p^3\ ^3D^o_2$	$2s^22p^2\ ^1D_2$	532703 (0.048)	3.827E+07 (6.27)
$2s2p^3\ ^3D^o_3$	$2s^22p^2\ ^1D_2$	558894 (0.049)	9.767E+08 (3.61)
$2s2p^3\ ^3P^o_1$	$2s^22p^2\ ^1D_2$	680356 (0.051)	2.577E+08 (2.44)
$2s2p^3\ ^3P^o_2$	$2s^22p^2\ ^1D_2$	697888 (0.052)	1.435E+08 (4.80)
$2s2p^3\ ^3S^o_1$	$2s^22p^2\ ^1D_2$	851344 (0.084)	3.607E+08 (3.16)
$2s2p^3\ ^1D^o_2$	$2s^22p^2\ ^1D_2$	882963 (0.037)	4.485E+10 (0.37)
$2s2p^3\ ^1P^o_1$	$2s^22p^2\ ^1D_2$	1016862 (0.170)	6.583E+10 (0.15)
$2s2p^3\ ^3D^o_1$	$2s^22p^2\ ^1S_0$	404698 (0.165)	4.070E+07 (2.97)
$2s2p^3\ ^3P^o_1$	$2s^22p^2\ ^1S_0$	552971 (0.014)	1.492E+08 (7.10)
$2s2p^3\ ^3S^o_1$	$2s^22p^2\ ^1S_0$	723959 (0.008)	6.511E+08 (2.13)
$2s2p^3\ ^1P^o_1$	$2s^22p^2\ ^1S_0$	889477 (0.147)	1.727E+10 (0.52)
$2p^4\ ^3P_2$	$2s2p^3\ ^5S^o_2$	1159940 (0.180)	1.422E+09 (2.39)
$2p^4\ ^3P_1$	$2s2p^3\ ^5S^o_2$	1254085 (0.181)	2.381E+08 (3.65)
$2p^4\ ^1D_2$	$2s2p^3\ ^5S^o_2$	1331255 (0.201)	5.282E+07 (2.48)
$2p^4\ ^3P_2$	$2s2p^3\ ^3D^o_1$	869710 (0.102)	3.455E+09 (0.75)
$2p^4\ ^3P_0$	$2s2p^3\ ^3D^o_1$	959080 (0.137)	3.474E+10 (0.43)
$2p^4\ ^3P_1$	$2s2p^3\ ^3D^o_1$	963855 (0.102)	1.434E+10 (0.27)
$2p^4\ ^1D_2$	$2s2p^3\ ^3D^o_1$	1041025 (0.103)	4.033E+06 (20.67)
$2p^4\ ^1S_0$	$2s2p^3\ ^3D^o_1$	1271738 (0.137)	2.331E+08 (1.32)
$2p^4\ ^3P_2$	$2s2p^3\ ^3D^o_2$	869090 (0.103)	1.335E+10 (0.00)
$2p^4\ ^3P_1$	$2s2p^3\ ^3D^o_2$	963235 (0.104)	2.124E+10 (0.28)
$2p^4\ ^1D_2$	$2s2p^3\ ^3D^o_2$	1040406 (0.106)	7.878E+08 (0.20)
$2p^4\ ^3P_2$	$2s2p^3\ ^3D^o_3$	842899 (0.137)	2.822E+10 (0.53)
$2p^4\ ^1D_2$	$2s2p^3\ ^3D^o_3$	1014215 (0.260)	5.622E+09 (0.85)
$2p^4\ ^3P_1$	$2s2p^3\ ^3P^o_0$	824204 (0.038)	4.813E+09 (0.02)
$2p^4\ ^3P_2$	$2s2p^3\ ^3P^o_1$	721437 (0.039)	3.678E+09 (0.32)
$2p^4\ ^3P_0$	$2s2p^3\ ^3P^o_1$	810807 (0.040)	1.827E+10 (0.93)
$2p^4\ ^3P_1$	$2s2p^3\ ^3P^o_1$	815582 (0.043)	1.273E+08 (3.29)
$2p^4\ ^1D_2$	$2s2p^3\ ^3P^o_1$	892752 (0.085)	1.241E+09 (1.85)
$2p^4\ ^1S_0$	$2s2p^3\ ^3P^o_1$	1123465 (0.233)	4.222E+09 (1.30)
$2p^4\ ^3P_2$	$2s2p^3\ ^3P^o_2$	703905 (0.039)	3.629E+09 (0.88)
$2p^4\ ^3P_1$	$2s2p^3\ ^3P^o_2$	798050 (0.040)	1.598E+10 (0.75)
$2p^4\ ^1D_2$	$2s2p^3\ ^3P^o_2$	875220 (0.085)	2.512E+09 (1.79)
$2p^4\ ^3P_2$	$2s2p^3\ ^3S^o_1$	550450 (0.021)	6.005E+09 (0.76)
$2p^4\ ^3P_0$	$2s2p^3\ ^3S^o_1$	639819 (0.020)	1.733E+10 (0.28)
$2p^4\ ^3P_1$	$2s2p^3\ ^3S^o_1$	644594 (0.049)	1.290E+10 (0.00)
$2p^4\ ^1D_2$	$2s2p^3\ ^3S^o_1$	721764 (0.059)	7.002E+06 (0.68)
$2p^4\ ^1S_0$	$2s2p^3\ ^3S^o_1$	952477 (0.060)	5.111E+09 (0.25)
$2p^4\ ^3P_2$	$2s2p^3\ ^1D^o_2$	518830 (0.065)	7.538E+08 (1.85)
$2p^4\ ^3P_1$	$2s2p^3\ ^1D^o_2$	612975 (0.124)	3.767E+08 (3.31)
$2p^4\ ^1D_2$	$2s2p^3\ ^1D^o_2$	690145 (0.311)	3.182E+10 (0.28)
$2p^4\ ^3P_2$	$2s2p^3\ ^1P^o_1$	384932 (0.274)	8.409E+07 (3.44)
$2p^4\ ^3P_0$	$2s2p^3\ ^1P^o_1$	474302 (0.271)	9.885E+06 (20.99)
$2p^4\ ^3P_1$	$2s2p^3\ ^1P^o_1$	479076 (0.265)	6.387E+08 (1.58)
$2p^4\ ^1D_2$	$2s2p^3\ ^1P^o_1$	556247 (0.139)	4.499E+09 (1.15)
$2p^4\ ^1S_0$	$2s2p^3\ ^1P^o_1$	786959 (0.156)	7.549E+10 (0.09)

Table 10. Transition rates for Ne-like S. A_{RCI} transition rates from RMCDHF/RCI [43], A_{BP} transition rates from multiconfiguration Hartree-Fock-Breit-Pauli [19] and A_{CIV3} transition rates from CI calculations using CIV3 [64].

States		ΔE (cm^{-1})	Type	A_{RCI}	A_{BP}	A_{CIV3}
Upper	**Lower**					
S VII						
$2p^5 3s\ ^3P^o_2$	$2p^6\ ^1S_0$	1371667	M2	7.638E+02	7.617E+02	
$2p^5 3s\ ^3P^o_1\ 0.81 + 0.18\ ^1P^o_1$	$2p^6\ ^1S_0$	1376084	E1	1.855E+10	1.816E+10	1.989E+10
$2p^5 3s\ ^1P^o_1\ 0.81 + 0.18\ ^3P^o_1$	$2p^6\ ^1S_0$	1388242	E1	8.421E+10	8.507E+10	8.777E+10
$2p^5 3p\ ^3D_2\ 0.79 + 0.16\ ^1D_2$	$2p^6\ ^1S_0$	1484530	E2	3.021E+06	2.964E+06	
$2p^5 3p\ ^3P_2\ 0.56 + 0.42\ ^1D_2$	$2p^6\ ^1S_0$	1492576	E2	8.028E+06	8.008E+06	
$2p^5 3d\ ^3P^o_1$	$2p^6\ ^1S_0$	1624769	E1	2.160E+09	2.182E+09	2.312E+09
$2p^5 3d\ ^3P^o_2$	$2p^6\ ^1S_0$	1627240	M2	1.710E+04	1.728E+04	
$2p^5 3d\ ^3D^o_1$	$2p^6\ ^1S_0$	1644545	E1	6.122E+10	6.206E+10	6.230E+10
$2p^5 3d\ ^1P^o_1$	$2p^6\ ^1S_0$	1662346	E1	9.452E+11	9.448E+11	9.087E+11
$2p^5 3s\ ^3P^o_1\ 0.81 + 0.18\ ^1P^o_1$	$2p^5 3s\ ^3P^o_2$	4417	M1	1.587E+00	1.601E+00	
$2p^5 3s\ ^1P^o_1\ 0.81 + 0.18\ ^3P^o_1$	$2p^5 3s\ ^3P^o_2$	16575	M1	1.849E+01	1.867E+01	
$2p^5 3p\ ^3S_1$	$2p^5 3s\ ^3P^o_2$	95373	E1	6.393E+08	6.504E+08	6.480E+08
$2p^5 3p\ ^3D_3$	$2p^5 3s\ ^3P^o_2$	111609	E1	1.566E+09	1.608E+09	1.594E+09
$2p^5 3p\ ^3D_2\ 0.79 + 0.16\ ^1D_2$	$2p^5 3s\ ^3P^o_2$	112863	E1	6.439E+08	6.627E+08	6.418E+08
$2p^5 3p\ ^3D_1\ 0.72 + 0.17\ ^1P_1$	$2p^5 3s\ ^3P^o_2$	116432	E1	1.994E+08	2.060E+08	2.023E+08
$2p^5 3p\ ^3P_2\ 0.56 + 0.42\ ^1D_2$	$2p^5 3s\ ^3P^o_2$	120909	E1	1.000E+09	1.031E+09	1.006E+09
$2p^5 3p\ ^1P_1\ 0.55 + 0.27\ ^3D_1$	$2p^5 3s\ ^3P^o_2$	124214	E1	7.124E+07	7.315E+07	6.807E+07
$2p^5 3p\ ^1D_2\ 0.42 + 0.38\ ^3P_2$	$2p^5 3s\ ^3P^o_2$	127448	E1	2.464E+08	2.501E+08	2.832E+08
$2p^5 3p\ ^3S_1$	$2p^5 3s\ ^1P^o_1\ 0.81 + 0.18\ ^3P^o_1$	78797	E1	1.188E+07	1.206E+07	1.253E+07
$2p^5 3p\ ^3D_2\ 0.79 + 0.16\ ^1D_2$	$2p^5 3s\ ^1P^o_1\ 0.81 + 0.18\ ^3P^o_1$	96287	E1	6.945E+06	7.197E+06	5.508E+06
$2p^5 3p\ ^3D_1\ 0.72 + 0.17\ ^1P_1$	$2p^5 3s\ ^1P^o_1\ 0.81 + 0.18\ ^3P^o_1$	99856	E1	3.825E+06	4.290E+06	4.536E+06
$2p^5 3p\ ^3P_2\ 0.56 + 0.42\ ^1D_2$	$2p^5 3s\ ^1P^o_1\ 0.81 + 0.18\ ^3P^o_1$	104333	E1	2.932E+08	2.977E+08	3.152E+08
$2p^5 3p\ ^1P_1\ 0.55 + 0.27\ ^3D_1$	$2p^5 3s\ ^1P^o_1\ 0.81 + 0.18\ ^3P^o_1$	107638	E1	7.415E+08	7.625E+08	7.557E+08

Table 10. *Cont.*

States				ΔE (cm^{-1})	Type	A_{RCI}	A_{BP}	A_{CIV3}
Upper		**Lower**						
$2p^5 3p\ ^3P_0$		$2p^5 3s\ ^1P_1^o$	$0.81 + 0.18\ ^3P_1^o$	110460	E1	1.908E+08	1.974E+08	2.006E+08
$2p^5 3p\ ^1D_2$	$0.42 + 0.38\ ^3P_2$	$2p^5 3s\ ^1P_1^o$	$0.81 + 0.18\ ^3P_1^o$	110872	E1	1.206E+09	1.243E+09	1.199E+09
$2p^5 3p\ ^3P_1$	$0.70 + 0.27\ ^1P_1$	$2p^5 3s\ ^1P_1^o$	$0.81 + 0.18\ ^3P_1^o$	112070	E1	7.082E+08	7.307E+08	7.000E+08
$2p^5 3p\ ^3P_1$	$0.70 + 0.27\ ^1P_1$	$2p^5 3s\ ^1P_1^o$	$0.81 + 0.18\ ^3P_1^o$	112070	M2	1.139E−01	1.191E−01	
$2p^5 3p\ ^1S_0$		$2p^5 3s\ ^1P_1^o$	$0.81 + 0.18\ ^3P_1^o$	165149	E1	5.082E+09	5.118E+09	5.073E+09
$2p^5 3d\ ^3P_1^o$		$2p^5 3p\ ^1D_2$	$0.42 + 0.38\ ^3P_2$	125654	E1	1.229E+08	1.235E+08	1.323E+08
$2p^5 3d\ ^3P_2^o$		$2p^5 3p\ ^1D_2$	$0.42 + 0.38\ ^3P_2$	128125	E1	3.010E+08	3.017E+08	3.358E+08
$2p^5 3d\ ^3P_2^o$		$2p^5 3p\ ^1D_2$	$0.42 + 0.38\ ^3P_2$	128125	M2	1.161E−01	1.175E−01	
$2p^5 3d\ ^3F_3^o$	$0.77 + 0.20\ ^1F_3^o$	$2p^5 3p\ ^1D_2$	$0.42 + 0.38\ ^3P_2$	132832	E1	1.471E+06	1.472E+06	1.078E+06
$2p^5 3d\ ^3F_2^o$	$0.71 + 0.17\ ^1D_2^o$	$2p^5 3p\ ^1D_2$	$0.42 + 0.38\ ^3P_2$	136157	E1	1.190E+06	1.370E+06	1.643E+06
$2p^5 3d\ ^1F_3^o$	$0.53 + 0.40\ ^3D_3^o$	$2p^5 3p\ ^1D_2$	$0.42 + 0.38\ ^3P_2$	138763	E1	1.511E+08	1.519E+08	1.131E+08
$2p^5 3d\ ^3D_1^o$		$2p^5 3p\ ^1D_2$	$0.42 + 0.38\ ^3P_2$	145430	E1	3.071E+06	3.159E+06	1.717E+06
$2p^5 3d\ ^1D_2^o$	$0.52 + 0.28\ ^3F_2^o$	$2p^5 3p\ ^1D_2$	$0.42 + 0.38\ ^3P_2$	145447	E1	6.172E+08	6.286E+08	6.276E+08
$2p^5 3d\ ^3D_3^o$	$0.57 + 0.27\ ^1F_3^o$	$2p^5 3p\ ^1D_2$	$0.42 + 0.38\ ^3P_2$	146716	E1	4.030E+09	4.093E+09	4.183E+09
$2p^5 3d\ ^3D_3^o$	$0.57 + 0.27\ ^1F_3^o$	$2p^5 3p\ ^1D_2$	$0.42 + 0.38\ ^3P_2$	146716	M2	1.029E+00	1.054E+00	
$2p^5 3d\ ^3D_2^o$	$0.65 + 0.27\ ^1D_2^o$	$2p^5 3p\ ^1D_2$	$0.42 + 0.38\ ^3P_2$	147358	E1	1.521E+08	1.531E+08	1.489E+08
$2p^5 3d\ ^1P_1^o$		$2p^5 3p\ ^1D_2$	$0.42 + 0.38\ ^3P_2$	163231	E1	4.854E+07	4.851E+07	5.550E+07

5.3. Systematic Comparisons between Methods

Wang and co-workers have systematically compared large sets of transition rates from accurate RMCDHF/RCI and RMBPT calculations [49–52]. These comparisons show that the rates from the two methods agree within a few percent for the strong transitions and that the agreement gets slightly worse for the weak intercombination and the two-electron, one photon transitions [1]. The comparisons also show that the differences between the methods are large for transitions for which there are large differences between the rates in the length and velocity form, thus confirming the usefulness of $\delta A/A$ as an uncertainty estimate. In Figure 3, we show the results of a comparison between methods for O-like Fe [31]. The figure clearly shows the consistency of the RMCDHF/RCI and RMBPT transitions rates, but also the comparatively large differences with rates from the CHIANTI database. These types of comparisons point to the fact that transition rates can be computed with high accuracy, but that much effort remains in order to make data practically available for astronomers and astrophysicist in updated databases.

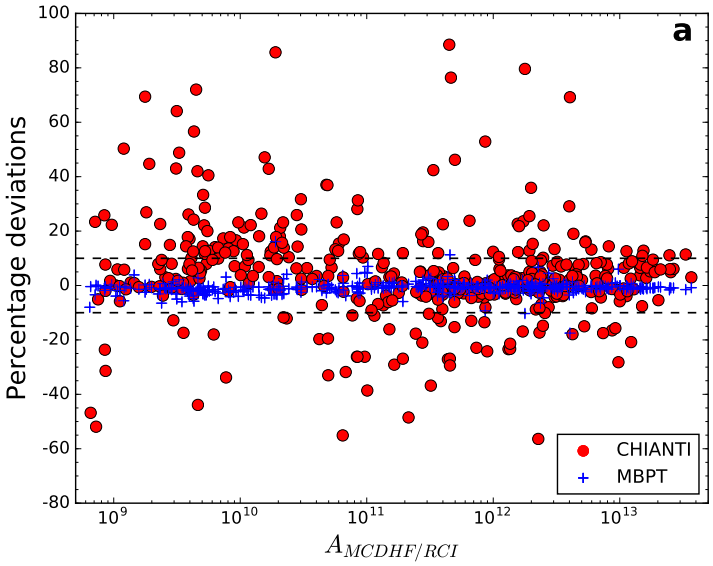

Figure 3. Results of a comparison between methods for O-like Fe [31]. Deviation in percent between RMCDHF/RCI and RMBPT transition rates as a function of the transition rate in s^{-1}. Deviations from the values of the CHIANTI database [3,4] are given in red. The dashed lines give the 10% levels.

6. Conclusions

Current computational methodologies make it possible to compute excitation and transition energies to almost spectroscopic accuracy for many ionized systems. In an astrophysical context, this means that calculated transition energies can be used to unambiguously identify new lines from spectra or correct old identifications. Transition data are lacking for many ions, and calculated values fill this gap. Whereas many of the calculations have been done for systems with relatively few electrons with a full RCI matrix, zero- and first-order methods, allowing for parts of the interactions to be treated perturbatively, have extended the range of applicability, and many calculations with high accuracy are in progress for isoelectronic sequences starting from the third and fourth row of the periodic table.

Accurate and consistent transition rates are essential for collisional and radiative plasma modelling and for diagnostic purposes. Very few experimental data are available for the rates, and thus, the bulk of the data must be computed. The lack of experimental data means that internal validation of

[1] Transitions between two states for which the configurations differ by more than one electron. These transitions are zero in the lowest approximation and are induced by CSFs that enter the calculation to correct for electron correlation effects.

computed data becomes important. For accurate calculations that predict the energy structure at the per millelevel, the differences between E1 rates in the length and velocity forms can be used to estimate the uncertainties. Internal validation based on convergence analysis and agreement between rates in length and velocity, as well as systematic comparisons of rates from RMCDHF/RCI and RMBPT calculations show that the uncertainties of the E1 rates are at the level of a few percent for the strong transitions. For the weakest transitions, the uncertainties are higher and come with a more irregular pattern.

7. Further Developments and Outlook

The time for angular integration is a limiting factor for very large RCI calculations. This time can be cut down by regrouping CSFs from SD-MR expansions in blocks that can be represented symbolically. For example, in non-relativistic notation, $1s^2nsmp\ ^3P$ and $1s^2npmd\ ^3P$ with $n = 2, \ldots, 12$ and $m = 2, \ldots, 12$ represent two blocks where the angular integration between CSFs in the blocks, as well as between CSFs in the different blocks is independent of the principal quantum numbers or can be reduced to only a few cases. For large n and m, the reduction in computing time is substantial. Discussed already decades ago [65], it seems essential that these ideas are now broadly implemented in the generally available computer codes.

With angular integration being a negligible part of the computation comes the possibility to extend the orbital set to higher n. Currently, the orbitals are variationally determined on a grid in RMCDHF calculations. The variational determination is computationally costly, and it would be valuable to augment the variationally-determined orbitals with analytical orbitals or orbitals determined in simplified and fast procedures. Work along these lines is in progress.

Among the targeted systems for improved computer codes are the α-elements, including Mg, Si, Ca and the iron group elements Sc, Ti, Cr, Mn, Fe at lower ionization states. These elements are of key importance for stellar and galactic evolution studies [66].

Acknowledgments: Per Jönsson, Henrik Hartman, Jörgen Ekman and Tomas Brage acknowledge support from the Swedish Research Council under Contract 2015-04842. Laima Radziute is thankful for the high performance computing resources provided by the Information Technology Open Access Center of Vilnius University. Michel R. Godefroid acknowledges support from the Belgian F.R.S.-FNRS Fonds de la Recherche Scientifique under CDR J.0047.16.

Author Contributions: All authors contributed equally to the work presented here.

Conflicts of Interest: The authors declare no conflict of interest.

References

1. Editorial. Nailing fingerprints in the stars. *Nature* **2013**, *437*, 503.
2. Pradhan, A.K.; Nahar, S.N. *Atomic Astrophysics and Spectroscopy*; Cambridge University Press: Cambridge, UK, 2011.
3. Dere, K.P.; Landi, E.; Mason, H.E.; Monsignori Fossi, B.C.; Young, P.R. CHIANTI—An atomic database for emission lines—Paper I: wavelengths greater than 50 Å (Version 1). *Astron. Astrophys. Suppl. Ser.* **1997**, *125*, 149–173.
4. Landi, E.; Young, P.R.; Dere, K.P.; Del Zanna, G.; Mason, H.E. CHIANTI—An atomic database for emission lines. XIII. Soft X-ray improvements and other changes: Version 7.1 of the database. *Astrophys. J.* **2013**, *763*, 86.
5. Del Zanna, G. Benchmarking atomic data for astrophysics: A first look at the soft X-ray lines. *Astron. Astrophys.* **2012**, *546*, A97.
6. Edlén, B. Atomic Spectra. *Encyclopedia of Physics*; Flügge, S., Ed.; Springer-Verlag: Berlin, Germany, 1964.
7. Froese Fischer, C.; Godefroid, M.; Brage, T.; Jönsson, P.; Gaigalas, G. Advanced multiconfiguration methods for complex atoms: Part I—Energies and wave functions. *J. Phys. B At. Mol. Opt. Phys.* **2016**, *49*, 182004.
8. Froese Fischer, C.; Brage, T.; Jönsson, P. *Computational Atomic Structure—An MCHF Approach*; CRC Press: Boca Raton, FL, USA, 1997.

9. Kozlov, M.G.; Porsev, S.G.; Safronova, M.S.; Tupitsyn, I.I. CI-MBPT: A package of programs for relativistic atomic calculations based on a method combining configuration interaction and many-body perturbation theory. *Comput. Phys. Commun.* **2015**, *195*, 199–213.
10. Verdebout, S.; Rynkun, P.; Jönsson, P.; Gaigalas, G.; Froese Fischer, C.; Godefroid, M. A partitioned correlation function interaction approach for describing electron correlation in atoms. *J. Phys. B At. Mol. Opt. Phys.* **2013**, *46*, 085003.
11. Dzuba, V.A.; Berengut, J.; Harabati, C.; Flambaum, V.V. Combining configuration interaction with perturbation theory for atoms with large number of valence electrons. *Phys. Rev. A* **2016**, *95*, 012503.
12. Gustafsson, S.; Jönsson, P.; Froese Fischer, C.; Grant, I.P. Combining Multiconfiguration and Perturbation Methods: Perturbative Estimates of Core–Core Electron Correlation Contributions to Excitation Energies in Mg-Like Iron. *Atoms* **2017**, *5*, 3.
13. Radžiūtė, L.; Gaigalas, G.; Kato, D; Jönsson, P.; Rynkun, P.; Kučas, S.; Jonauskas, V.; Matulianec, R. Energy level structure of Er^{3+}. *J. Quant. Spectrosc. Radiat. Transf.* **2015**, *152*, 94–106.
14. Jönsson, P.; Gaigalas, G.; Bieroń, J.; Froese Fischer, C.; Grant, I.P. New Version: grasp2K relativistic atomic structure package. *Comput. Phys. Commun.* **2013**, *184*, 2197–2203.
15. Grant, I.P. *Relativistic Quantum Theory of Atoms and Molecules*; Springer: New York, NY, USA; 2007.
16. Dyall, K.G.; Grant, I.P.; Johnson, C.T.; Parpia, F.A.; Plummer, E.P. GRASP: A general-purpose relativistic atomic structure program. *Comput. Phys. Commun.* **1989**, *55*, 425–456.
17. Grant, I.P.; Pyper, N.C. Breit-interaction in multi-configuration relativistic atomic calculations. *J. Phys. B* **1976**, *9*, 761–774.
18. Gaigalas, G.; Žalandauskas, T.; Rudzikas, Z. LS-jj transformation matrices for a shell of equivalent electrons. *At. Data Nucl. Data Tables* **2003**, *84*, 99–190.
19. Froese Fischer, C.; Tachiev, G. Breit-Pauli energy levels, lifetimes, and transition probabilities for the beryllium-like to neon-like sequences. *At. Data Nucl. Data Tables* **2004**, *87*, 1–184.
20. Froese Fischer, C.; Gaigalas, G. Multiconfiguration Dirac-Hartree-Fock energy levels and transition probabilities for W XXXVIII. *Phys. Rev. A* **2012**, *85*, 042501.
21. Gaigalas, G.; Froese Fischer, C.; Rynkun, P.; Jönsson, P. JJ2LSJ transformation and unique labeling for energy levels. *Atoms* **2017**, *5*, 6.
22. Gaigalas, G.; Rudzikas, Z.; Froese Fischer, C. An efficient approach for spin-angular integrations in atomic structure calculations. *J. Phys. B At. Mol. Opt. Phys.* **1997**, *30*, 3747–3771.
23. Gaigalas, G.; Fritzsche, S.; Grant, I.P. Program to calculate pure angular momentum coefficients in jj-coupling. *Comput. Phys. Commun.* **2001**, *139*, 263–278.
24. Olsen, J.; Godefroid, M.; Jönsson, P.; Malmqvist, P.Å.; Froese Fischer, C. Transition probability calculations for atoms using nonorthogonal orbitals. *Phys. Rev. E* **1995**, *52*, 4499–4508.
25. Jönsson, P.; Froese Fischer, C. Multiconfiguration Dirac-Fock calculations of the $2s^2\ {}^1S_0 - 2s2p\ {}^3P_1$ intercombination transition in C III. *Phys. Rev. A* **1998**, *57*, 4967–4970.
26. Grant, I.P. Gauge invariance and relativistic radiative transitions. *J. Phys. B At. Mol. Phys.* **1974**, *7*, 1458–1475.
27. Froese Fischer, C.; Gaigalas, G.; Jönsson, P. Core effects on transition energies for $3d^k$ configurations in Tungsten ions. *Atoms* **2017**, *5*, 7.
28. Rynkun, P.; Jönsson, P.; Gaigalas, G. Energies and E1, M1, E2, M2 transition rates for states of the $2s^22p$, $2s2p^2$, and $2p^3$ configurations in boron-like ions between N III and Zn XXVI. *At. Data Nucl. Data Tables* **2012**, *98*, 481–556.
29. Jönsson, P.; Rynkun, P.; Gaigalas, G. Energies, E1, M1, and E2 transition rates, hyperfine structures, and Landé g_J factors for the states of the $2s^22p^2$, $2s2p^3$, and $2p^4$ configurations in carbon-like ions between F IV and Ni XXIII. *At. Data Nucl. Data Tables* **2011**, *97*, 648–691.
30. Rynkun, P.; Jönsson, P.; Gaigalas, G.; Froese Fischer, C. Energies and E1, M1, E2, and M2 transition rates for states of the $2s^22p^3$, $2s2p^4$, and $2p^5$ configurations in nitrogen-like ions between F III and Kr XXX. *At. Data Nucl. Data Tables* **2014**, *100*, 315–402.
31. Rynkun, P.; Jönsson, P.; Gaigalas, G.; Froese Fischer, C. Energies and E1, M1, E2, and M2 transition rates for states of the $2s^22p^4$, $2s2p^5$, and $2p^6$ configurations in oxygen-like ions between F II and Kr XXIX. *Astron. Astrophys.* **2013**, *557*, A136.

32. Jönsson, P.; Alkauskas, A.; Gaigalas, G. Energies and E1, M1, E2 transition rates for states of the $2s^2 2p^5$ and $2s2p^6$ configurations in fluorine-like ions between Si VI and W LXVI. *At. Data Nucl. Data Tables* **2013**, *99*, 431–446.
33. Nazé, C.; Verdebout, S.; Rynkun, P.; Gaigalas, G.; Godefroid, M.; Jönsson, P. Isotope shifts in beryllium-, boron-, carbon-, and nitrogen-like ions from relativistic configuration interaction calculations. *At. Data Nucl. Data Tables* **2014**, *100*, 1197–1249.
34. Verdebout, S., Nazé, C.; Jönsson, P.; Rynkun, P.; Godefroid, M.; Gaigalas, G. Hyperfine structures and Landé g_J-factors for $n = 2$ states in beryllium-, boron-, carbon-, and nitrogen-like ions from relativistic configuration interaction calculations. *At. Data Nucl. Data Tables* **2014**, *100*, 1111–1155.
35. Kelly, R.L. Atomic and Ionic Spectrum Lines Below 2000 Angstroms: Hydrogen Through Krypton. *J. Phys. Chem. Ref. Data Suppl.* **1987**, *16*, 1–1698.
36. Edlén, B. Comparison of Theoretical and Experimental Level Values of the n = 2 Complex in Ions Isoelectronic with Li, Be, O and F. *Phys. Scr.* **1983**, *28*, 51–67.
37. Kramida, A.E.; Ralchenko, Y.; Reader, J.; NIST ASD Team (2015). NIST Atomic Spectra Database (ver. 5.3). National Institute of Standards and Technology: Gaithersburg, MD. Available online: http://physics.nist.gov/asd (accessed on 28 December 2016).
38. Vilkas, M.J.; Ishikawa, Y.; Koc, K. Relativistic multireference many-body perturbation theory for quasidegenerate systems: Energy levels of ions of the oxygen isoelectronic sequence. *Phys. Rev. A* **1999**, *60*, 2808–2821.
39. Gaigalas, G.; Kaniauskas, J.; Kisielius, R.; Merkelis, G.; Vilkas, M.J. Second-order MBPT results for the oxygen isoelectronic sequence. *Phys. Scr.* **1994**, *49*, 135–147.
40. Bhatia, A.K.; Thomas, R.J.; Landi, E. Atomic data and spectral line intensities for Ne III. *At. Data Nucl. Data Tables* **2003**, *83*, 113–152.
41. Jonauskas, V.; Keenan, F.P.; Foord, M.E.; Heeter, R.F.; Rose, S.J.; Ferland, G.J.; Kisielius, R.; van Hoof, P.A.M.; Norrington, P.H. Dirac-Fock energy levels and transition probabilities for oxygen-like Fe XIX. *Astron. Astrophys.* **2004**, *424*, 363–369.
42. Landi, E.; Gu, M.F. Atomic Data for High-Energy Configurations in Fe XVII-XXIII. *Astrophys. J.* **2006**, *640*, 1171–1179.
43. Jönsson, P.; Bengtsson, P.; Ekman, J.; Gustafsson, S.; Karlsson, L.B.; Gaigalas, G.; Froese Fischer, C.; Kato, D.; Murakami, I.; Sakaue, H.A.; et al. Relativistic CI calculations of spectroscopic data for the $2p^6$ and $2p^5 3l$ configurations in Ne-like ions between Mg III and Kr XXVII. *At. Data Nucl. Data Tables* **2014**, *100*, 1–154.
44. Ishikawa, Y.; Lopez Encarnacion, J.M.; Träbert, E. $N = 3 - 3$ transitions of Ne-like ions in the iron group, especially Ca $^{10+}$ and Ti $^{12+}$. *Phys. Scr.* **2009**, *79*, 025301.
45. Jönsson, P.; Ekman, J.; Gustafsson, S.; Hartman, H.; Karlsson, L.B.; du Rietz, R.; Gaigalas, G.; Godefroid, M.R.; Froese Fischer, C. Energy levels and transition rates for the boron isoelectronic sequence: Si X, Ti XVIII – Cu XXV. *Astron. Astrophys.* **2013**, *559*, A100.
46. Jönsson, P.; Ekman, J.; Träbert, E. MCDHF Calculations and Beam-Foil EUV Spectra of Boron-like Sodium Ions (Na VII). *Atoms* **2015**, *3*, 195–259.
47. Ekman, J.; Jönsson, P.; Gustafsson, S.; Hartman, H.; Gaigalas, G.; Godefroid, M.R.; Froese Fischer, C. Calculations with spectroscopic accuracy: Energies, Landé g_J-factors, and transition rates in the carbon isoelectronic sequence from Ar XIII to Zn XXV. *Astron. Astrophys.* **2014**, *564*, A24.
48. Radžiūtė, L.; Ekman, J.; Jönsson P.; Gaigalas, G. Extended calculations of level and transition properties in the nitrogen isoelectronic sequence: Cr XVIII, Fe XX, Ni XXII, and Zn XXIV. *Astron. Astrophys.* **2015**, *582*, A61.
49. Wang, K.; Guo, X.L.; Li, S.; Si, R.; Dang, W.; Chen, Z.B.; Jönsson, P.; Hutton, R.; Chen, C.Y.; Yan, J. Calculations with spectroscopic accuracy: Energies and transition rates in the nitrogen isoelectronic sequence from Ar XII to Zn XXIV. *Astrophys. J. Suppl.* **2016**, *223*, 3.
50. Wang, K.; Jönsson, P.; Ekman, J.; Gaigalas, G.; Godefroid, M.R.; So, R.; Chen, Z.B.; Li, S.; Chen, C.Y.; Yan, J. Extended Calculations of Spectroscopic Data Energy Levels, Lifetimes and Transition Rates for O-like Ions from Cr XVII to Zn XXIII. *Astrophys. J. Suppl.* **2017**, *229*, 37.
51. Si, R.; Li, S.; Guo, X.L.; Chen, Z.B.; Brage, T.; Jönsson, P.; Wang, K.; Yan, J.; Chen, C.Y.; Zou, Y.M. Extended calculations with spectroscopic accuracy: energy levels and transition properties for the fluorine isoelectronic sequence with $Z = 24 - 30$. *Astrophys. J. Suppl.* **2016**, *227*, 16.

52. Wang, K.; Chen, Z.B.; Si, R.; Jönsson, P.; Ekman, J.; Guo, X.L.; Li, S.; Long, F.Y.; Dang, W.; Zhao, X.H.; et al. Extended relativistic configuration interaction and many-body perturbation calculations of spectroscopic data for the $n \leq 6$ configurations in Ne-like ions between Cr XV and Kr XXVII. *Astrophys. J. Suppl.* **2016**, *226*, 14.
53. Gu, M.F. Wavelengths of $2l \rightarrow 3l'$ transitions in L-shell ions of iron and nickel: A combined configuration interaction and many-body perturbation approach. *Astrophys. J. Suppl.* **2005**, *156*, 105–110.
54. Gustafsson, S.; Jönsson, P.; Froese Fischer, C.; Grant, I.P. MCDHF and RCI calculations of energy levels, lifetimes and transition rates for $3l3l'$, $3l4l'$ and $3s5l$ states in Ca IX—As XXII and Kr XXV. *Astron. Astrophy* **2017**, *505*, A76.
55. Ekman, J.; Jönsson, P.; Radžiūtė, L.; Gaigalas, G.; Del Zanna, G.; Grant, I.P. Large-scale calculations of atomic level and transition properties in the aluminium isoelectronic sequence from Ti X through Kr XXIV, Xe XLII, and W LXII. *At. Data Nucl. Data Tables* **2017**, submitted.
56. Jönsson, P.; Radžiūtė, L.; Gaigalas, G.; Godefroid, M.R.; Marques, J.P.; Brage, T.; Froese Fischer, C.; Grant, I.P. Accurate multiconfiguration calculations of energy levels, lifetimes and transition rates for the silicon isoelectronic sequence: Ti IX—Ge XIX, Sr XXV, Zr XXVII, Mo XXIX. *Astron. Astrophys.* **2016**, *585*, A26.
57. Del Zanna, G. Benchmarking atomic data for astrophysics: Fe XIII EUV lines. *Astron. Astrophys.* **2011**, *533*, A12.
58. Vilkas, M.J.; Ishikawa, Y. High-accuracy calculations of term energies and lifetimes of silicon-like ions with nuclear charges $Z = 24 - 30$. *J. Phys. B At. Mol. Opt. Phys.* **2004**, *37*, 1803–1816.
59. Träbert, E. Critical Assessment of Theoretical Calculations of Atomic Structure and Transition Probabilities: An Experimenter's View. *Atoms* **2014**, *2*, 15–85.
60. Träbert, E.; Curtis, L.J. Isoelectronic trends of line strength data in the Li and Be isoelectronic sequences. *Phys. Scr.* **2006**, *74*, C46–C54.
61. Froese Fischer, C. Evaluating the accuracy of theoretical transition data. *Phys. Scr.* **2009**, *134*, 014019.
62. Ekman, J.; Godefroid, M.R.; Hartman, H. Validation and Implementation of Uncertainty Estimates of Calculated Transition Rates. *Atoms* **2014**, *2*, 215–224.
63. Ynnerman, A.; Froese Fischer, C. Multiconfigurational-Dirac-Fock calculation of the $2s\ ^1S_0 - 2s2p\ ^3P_1$ spin-forbidden transition for the Be-like isoelectronic sequence. *Phys. Rev. A* **1995**, *51*, 2020–2030.
64. Hibbert, A.; Ledourneuf, M.; Mohan, M. Energies, Oscillator Strengths, and Lifetimes for Neon-like Ions Up to Kr XXVII. *At. Data Nucl. Data Tables* **1993**, *53*, 23–112.
65. Froese Fischer, C.; Jönsson, P. MCHF calculations for atomic properties. *Comput. Phys. Commun.* **1994**, *84*, 37–58.
66. Pagel, B.E.J. *Nucleosynthesis and Chemical Evolution of Galaxies*; Cambridge University Press: Cambridge, UK, 2009.